



# Low-dimensional chaotic dynamics versus intrinsic stochastic noise: a paradigm model

A. Majda<sup>a,b</sup>, I. Timofeyev<sup>c,\*</sup>

<sup>a</sup> *Courant Institute of Mathematical Sciences, New York University, New York, NY 10012, USA*

<sup>b</sup> *Center for Atmosphere Ocean Science, New York University, New York, NY 10012, USA*

<sup>c</sup> *Department of Mathematics, University of Houston, Houston, TX 77204-3008, USA*

Received 10 October 2003; received in revised form 13 April 2004; accepted 1 May 2004

Communicated by I. Mezic

---

## Abstract

Several prototype models are introduced here which are designed to elucidate the interaction between heteroclinic low-dimensional chaos in the projected nonlinear dynamics and intrinsic stochasticity induced by energy exchange with a bath of fast variables. These models are built by coupling a four-dimensional ODE with known analytical properties including heteroclinic cycles with a suitable deterministic bath of fast variables. A systematic strategy for stochastic mode reduction is applied to these models with 104 degrees of freedom to derive four-dimensional reduced stochastic equations for the slow variables. Due to the internal chaotic dynamics of the slow variables the stochastic mode reduction strategy is very robust in this case and yields reduced models which accurately capture the statistical behavior of the original deterministic system. Furthermore, it is also shown here that even in the regime of a weak coupling between the slow variables and the fast heat bath, the detailed structure of the stochastic terms derived through the mode-elimination procedure is essential for reproducing the statistical behavior of the slow dynamics. © 2004 Published by Elsevier B.V.

*PACS:* 02.50-r; 02.70.Rw; 05.20.-y; 05.70.Ln

*Keywords:* Stochastic modeling; Mode reduction; Non-Gaussian statistics; Heteroclinic orbit

---

## 1. Introduction

During the last few decades a considerable attention has been given to the role of coherent structures in atmosphere/ocean modeling, turbulence, and other areas of nonlinear science. A dynamical systems approach and bifurcation theory has been applied with some success to low-dimensional truncations of complex models to ex-

---

\* Corresponding author. Tel.: +1 713 743 3483; fax: +1 713 743 3505.

*E-mail address:* [ilya@math.uh.edu](mailto:ilya@math.uh.edu) (I. Timofeyev).

Table 1  
Interaction coefficients for the “additive” model

|                       |                           |                           |
|-----------------------|---------------------------|---------------------------|
| $b^{x_1 u_1} = 1$     | $b^{v_1 x_1 w_1} = -0.75$ | $b^{w_1 x_1 v_1} = -0.25$ |
| $b^{y_1 u_1} = -0.7$  | $b^{v_1 y_1 w_1} = 1$     | $b^{w_1 y_1 v_1} = -0.3$  |
| $b^{x_2 u_2} = 1$     | $b^{v_2 x_2 w_2} = -0.6$  | $b^{w_2 x_2 v_2} = -0.4$  |
| $b^{y_2 u_2} = -0.55$ | $b^{v_2 y_2 w_2} = 1$     | $b^{w_2 y_2 v_2} = -0.45$ |

Table 2  
Additive Model with  $\lambda = 2$ ; one-point statistics of the slow variables computed from the DNS of the full system in (4) and reduced model in (8)

|                  | $x_1$     | $y_1$    | $x_2$     | $y_2$     |
|------------------|-----------|----------|-----------|-----------|
| Mean DNS         | -0.000991 | 0.000238 | -0.000631 | -0.016588 |
| Mean reduced     | 0.000902  | 0.000038 | 0.001741  | -0.017342 |
| Var DNS          | 0.01045   | 0.01057  | 0.01638   | 0.01638   |
| Var reduced      | 0.01049   | 0.01052  | 0.01607   | 0.01682   |
| Flatness DNS     | 2.1222    | 2.0514   | 2.4612    | 2.4886    |
| Flatness reduced | 2.1736    | 2.0612   | 2.4845    | 2.4507    |

plain complicated PDE phenomena. As regards the atmospheric sciences, this approach involves identifying stable structures such as multiple equilibria, periodic orbits or homoclinic/heteroclinic connections in the phase space of a low-dimensional projection [8,19,26,31,9,10] and then using observational or numerical data to search for the “ghost” of this behavior in the full complex dynamics [25]. Low-dimensional systems have also been introduced as simple prototype models of turbulent fluid boundary layers [4] and nonlinear optics [5]. In this approach, the

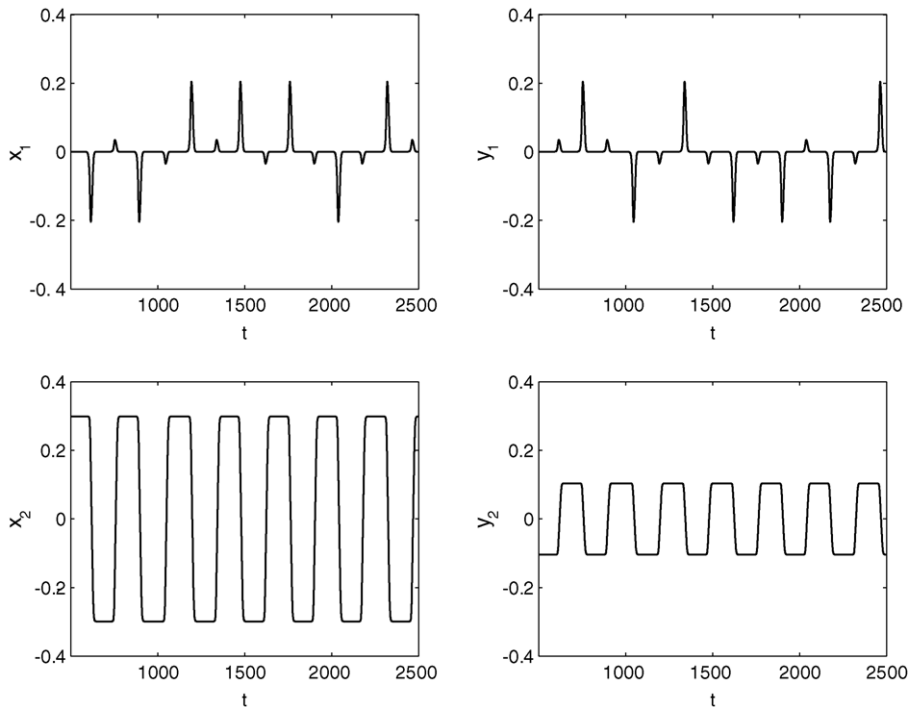


Fig. 1. Time series of  $z_1 = x_1 + iy_1$  and  $z_2 = x_2 + iy_2$  for the simulations of the uncoupled system in (1) in the regime with stable heteroclinic cycle.

analytically tractable chaotic behavior of these low-dimensional models is usually credited for the complex turbulent behavior of the full spatially extended systems [3,20]. Also, the effects of small random additive noises are often introduced to model interactions with neglected scales [12,23].

Stochastic modeling and reduction of degrees of freedom is another important research topic in modern nonlinear science. Often, the complexity of straightforward analytical models overwhelms computational capacity. To list a few, the dynamics of coupled atmosphere/ocean systems [39], simulations of macromolecular dynamics [17], or urban air-pollution studies [7]. The vast difference of time scales in the problem combined with large dimensionality is, usually, the main factor which prevents performing well-resolved direct numerical simulations. Low-dimensional reduced models where interactions with non-essential degrees of freedom are represented stochastically provide a computationally feasible alternative. This approach has been successfully utilized in atmosphere/ocean science starting with the pioneering work of Leith [30] and Hasselman [21]. Recent examples of reduced stochastic models include development of linear stochastic models for the low-frequency variability of the extra-tropical atmosphere [11,6,2,41], higher order Markov models for the angular momentum budget [14,15], and stochastic projection techniques combined with Markov jump processes for reduced models of macromolecular dynamics [40].

Most of the examples mentioned above adapt an ad-hoc modeling approach where the non-essential degrees of freedom are replaced by an assumed linear stochastic model of the additive type, and the unknown coefficients are regression-fit using numerical or observational data. An alternative systematic approach to stochastic mode-reduction has been recently developed by Vanden-Eijnden and the authors in [34,35]. This mode-elimination technique is a two-step procedure exploiting the assumption that the variables in the system under consideration can be split into two sets; a set of essential slow (resolved) variables, and a set of fast non-essential (unresolved) degrees of freedom. In the first step of the mode-elimination procedure the nonlinear self-interactions of the fast degrees of

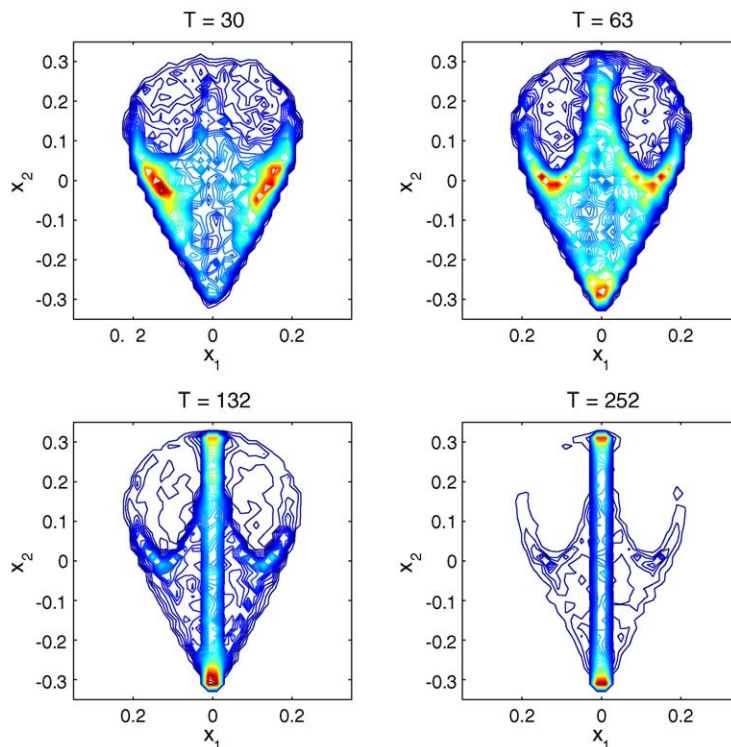


Fig. 2. Snapshots of the joint PDF  $x_1, x_2$  for the Monte-Carlo simulations of the system in (1).

freedom are represented stochastically. The motivation is that the self-interaction terms are responsible for the sensitive dependence on small perturbations in the system and can be represented stochastically if a coarse-grained description of the slow dynamics is the objective. In the second step of the procedure the fast unresolved degrees of freedom are eliminated from the equations utilizing standard adiabatic elimination techniques [27,29,18]. The adiabatic elimination is an asymptotic theory rigorous in the limit of infinite separation of time scales between the slow and fast degrees of freedom.

The advantages of the mode-elimination technique developed in [34,35] have been demonstrated in two recent papers [36,37]. Unlike most of the approaches mentioned in the above paragraph, the mode-elimination technique systematically gives the structure of stochastic terms in the reduced model of the slow dynamics. It has been demonstrated in [36,37] that multiplicative noises and nonlinear corrections play an important role in the nonlinear dynamics of the slow variables and that the strength of additive noises and linear damping can be predicted a priori by the theory. Another important practical issue is the separation of slow and fast variables in the system. The mode-elimination procedure works surprisingly well for models where unresolved degrees of freedom are roughly two times faster than the resolved ones and gives a qualitatively correct picture when the two time scales are the same. In [37] the important question of interplay between stable dynamical structures in the phase space of the resolved modes and stochastic terms was also addressed. Several special types of idealized systems were analyzed; each of them was carefully constructed to mimic potential applications in atmospheric science. Examples of such behavior include stable periodic motion and multiple equilibria in the truncated dynamics.

Recent interesting work for the low-frequency variability of the atmosphere [10,25] has suggested the role of heteroclinic cycles as a potential transition mechanism among atmospheric regimes. In these situations, non-trivial topography creates interactions which typically break the symmetries of heteroclinic cycles in a deterministic system

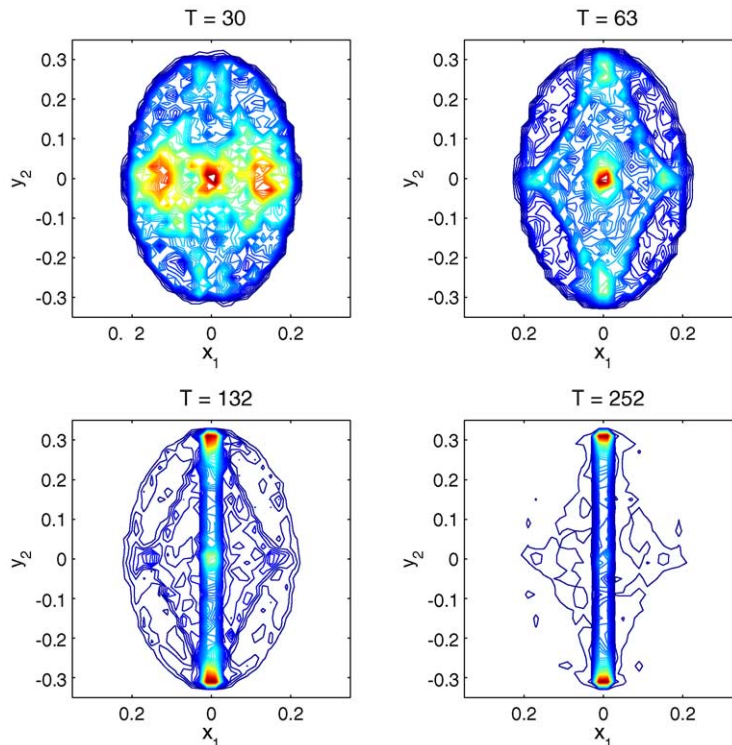


Fig. 3. Snapshots of the joint PDF  $x_1, y_2$  for the Monte-Carlo simulations of the system in (1).

with many degrees of freedom with additional chaos from the intrinsic stochastic noise due to back-scattering of turbulent cascades. Also for simple ocean models, various interesting low-dimensional chaotic regimes have been discovered recently with unrealistically high dissipation [13,38]. In more active mesoscale eddy resolving models, the competition between such chaotic dynamics and intrinsic stochastic noise from the turbulence becomes very interesting. Such effects are also likely to become prominent for midlatitude coupled atmosphere/ocean system. For these and other potential applications for atmosphere/ocean science as well as other scientific disciplines, it is interesting to develop unambiguous simplified models with both stable heteroclinic orbits in a truncated system and intrinsic stochastic noise through the back-scattering interaction with many turbulent chaotic degrees of freedom. The goal of the present work is to develop such a class of unambiguous models to address the question and to apply the systematic stochastic mode-reduction techniques described above [34–37] to study the role of truncated heteroclinic chaos in competition with intrinsic stochastic noise. Here the canonical system of four-dimensional ordinary differential equations (ODEs) with stable heteroclinic cycles arising from 2:1 resonance [3,22] is coupled to the Burgers–Hopf deterministic chaotic bath of modes [32,33,1] through a variety of energy conserving quadratic nonlinear interactions to define the basic models. The coupling breaks the original symmetry of the four-dimensional system; this situation is typical for geophysical fluid dynamics where low-dimensional projections typically have very special properties compared with the full dynamics. The four variables in the heteroclinic ODE naturally serve as slow resolved modes in the coupled systems and reduced stochastic differential equations are derived by the mode-elimination procedure. In all examples the statistical behavior of the four reduced modes in the direct numerical simulations of coupled systems with 104 degrees of freedom is compared with the statistics of the reduced systems obtained by mode-elimination to address the fundamental role of low-dimensional heteroclinic chaos coupled with intrinsic stochastic noise. In all the cases developed below, the agreement is excellent so the four mode reduced stochastic equations provide simplified models for the interaction of heteroclinic chaos with intrinsic stochastic noise.

The rest of the paper is organized as follows. In [Section 2](#) we introduce the model and discuss its analytical properties. In [Section 3](#) Monte-Carlo simulations of the four-dimensional dynamical system are performed and the

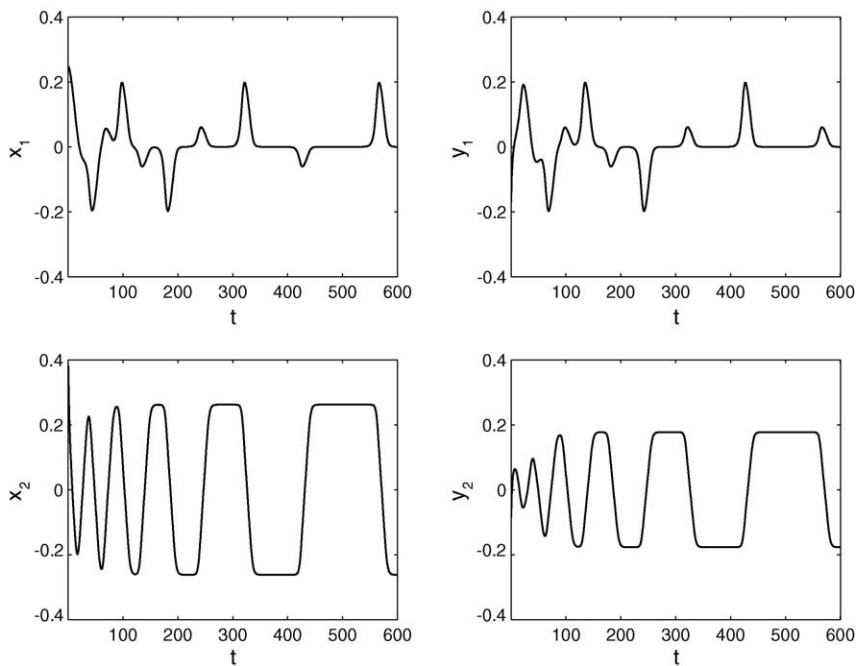


Fig. 4. Initial Transient Period in a single realization of the heteroclinic ODE in (1).

statistical behavior of ensembles is analyzed. In Section 4.1 we consider the first type of coupling. The heteroclinic system is coupled to the Burgers–Hopf bath in an additive fashion, leading to Langevin-type corrections to the heteroclinic ODE. Multiplicative coupling is analyzed in detail in Section 4.2. Multiplicative noises and nonlinear corrections arise in the reduced equations and it is also emphasized that even a weak coupling can have a drastic effect on the statistical behavior of the slow dynamics. Finally, in Section 5 behavior of an additive type model is analyzed as one of the parameters goes through the bifurcation sequence of the four-dimensional heteroclinic ODE.

## 2. The model

To investigate the interplay between low-dimensional heteroclinic chaos and intrinsic noise induced by the coupling with the fast unresolved modes with many degrees of freedom prototype models are built in a simple fashion. A four-dimensional system of ordinary differential equations with known dynamical properties including stable heteroclinic connections is coupled to a deterministic heat bath. The coupling is selected to mimic possible energy exchange scenarios in fluid dynamics; the interactions with the bath are constructed in an energy-preserving fashion, but they break the original  $O(2)$  symmetry of the heteroclinic ODE. The following four-dimensional system was shown to exhibit a wide variety of dynamical properties, including stable heteroclinic cycles [3,22]

$$\dot{z}_1 = z_1^* z_2 + (\mu_1 + e_{11}|z_1|^2 + e_{12}|z_2|^2)z_1, \quad \dot{z}_2 = -z_1^2 + (\mu_2 + e_{21}|z_1|^2 + e_{22}|z_2|^2)z_2. \quad (1)$$

The heat bath of unresolved modes is obtained by projecting the inviscid Burgers–Hopf equation  $u_t + uu_x = 0$  in periodic geometry on a finite number of Fourier coefficients. This truncated Burgers–Hopf model has been

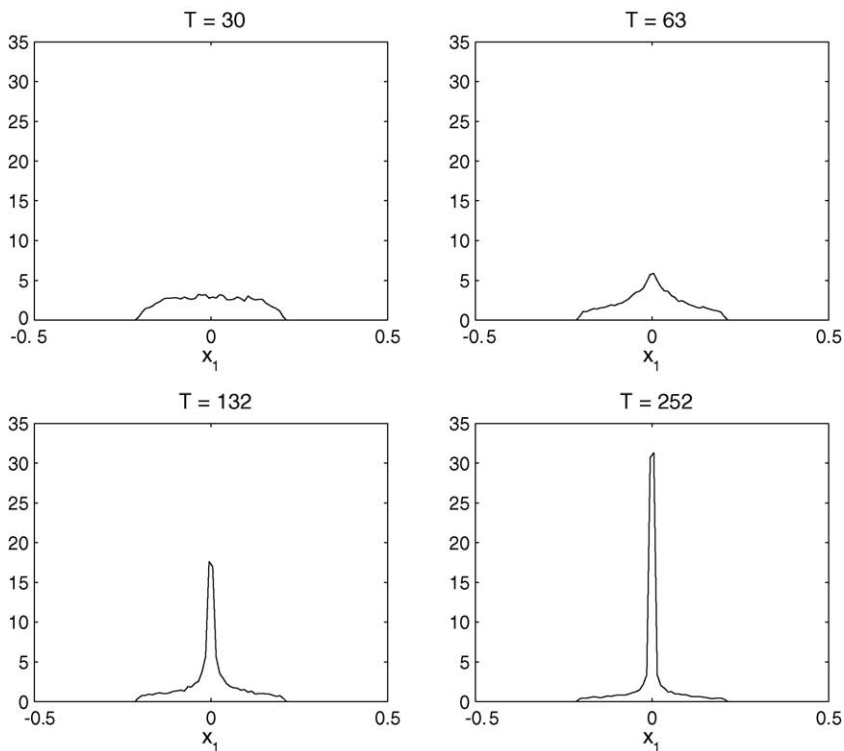


Fig. 5. Snapshots of the marginal PDF of  $x_1$  for the Monte-Carlo simulations of the system in (1).

investigated by the authors in a series of papers [32,33,1] and was shown to be highly chaotic and mixing and to obey a simple scaling relationship for auto-correlation functions. The equations for the Fourier coefficients of the expansion  $u = \sum \hat{u}_k e^{ikx}$ ,  $1 \leq |k| \leq \Lambda$  with  $\hat{u}_k^* = \hat{u}_{-k}$  read

$$\dot{v}_k = -\text{Re} \frac{ik}{2} \sum_{p+q+k=0} \hat{u}_p^* \hat{u}_q^*, \quad \dot{w}_k = -\text{Im} \frac{ik}{2} \sum_{p+q+k=0} \hat{u}_p^* \hat{u}_q^*, \tag{2}$$

where  $\hat{u}_k = v_k + iw_k$ . As in [32,33,1], the value  $\Lambda = 50$  is utilized below so that these are 100 modes in the heat bath. The paradigm models for the present study involve coupling the four modes in (1) with the 100 modes in (2) through simple energy conserving triad interactions which break the  $O(2)$  symmetry in (1).

The equations in (1) have been thoroughly analyzed in [3] and the bifurcation diagram has been mapped out. As parameters  $\mu_1$  and  $\mu_2$  change, the system goes through a series of bifurcations exhibiting a wide variety of dynamical regimes. In particular, as  $\mu_1$  is decreased, trivial solutions (fixed points) bifurcate to periodic solutions, then periodic cycles becomes unstable and the dynamics is dominated by modulated periodic solutions. If the parameter  $\mu_1$  is decreased further, stable heteroclinic orbits emerge which connect diametrically opposite points on the circle  $|z_2|^2 = -\mu_2/e_{22}$ ,  $z_1 = 0$ . The phase of these two points is a free parameter which is determined by the initial conditions in each particular realization. The stability of these orbits is guaranteed if  $\mu_1 - \mu_2 e_{12}/e_{22} < 0$  and  $\mu_2 > 0$ . Other solutions such as periodic orbits and modulated traveling waves may coexist with heteroclinic cycles, but become unstable. Fig. 1 shows time series of  $z_1$  and  $z_2$  for a typical simulation in the regime with a stable heteroclinic cycle. The values of the parameters utilized in this simulation are presented in (3). For this particular realization the two equilibria connected by a heteroclinic cycle are  $(z_1, z_2) = (0, 0, -0.3, 0.1)$  and  $(z_1, z_2) = (0, 0, 0.3, -0.1)$ .

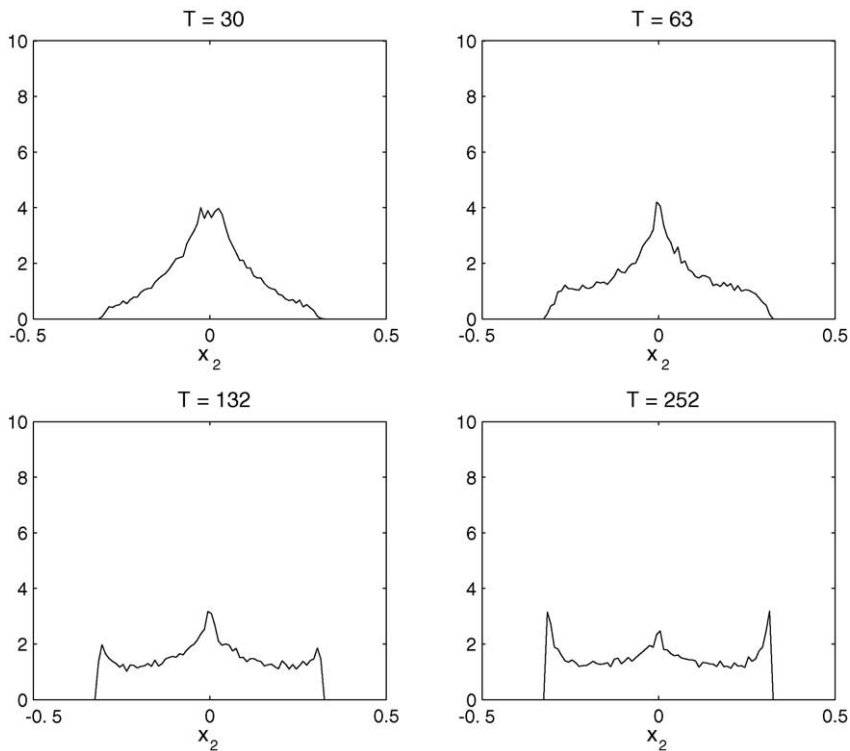


Fig. 6. Snapshots of the marginal PDF of  $x_2$  for the Monte-Carlo simulations of the system in (1)

When only the quadratic terms in (1) remain (i.e. all the free parameters are zero), the system becomes a pure 2:1 resonance interaction model. In this case the system in (1) conserves the energy  $E = |z_1|^2 + |z_2|^2$  and is, in fact, completely integrable (see, for example, [33]).

### 3. Statistical behavior of solutions of the heteroclinic ODE

When an attracting phase space structure such as a heteroclinic orbit is present, a generic solution of (1) has two dynamical stages. During the short first stage solutions are not close to a heteroclinic connection and follow paths which might be unstable, such as coexisting unstable periodic motion. Then, solutions are quickly attracted onto a heteroclinic cycle and follow an irregular pattern of bursts out of the  $z_1 = 0$  plane. Monte-Carlo simulations provide insight into the statistical behavior of ensembles of solutions for the uncoupled system in (1). The choice of parameters

$$\mu_1 = 0.05, \quad \mu_2 = 0.2, \quad e_{11} = -4, \quad e_{12} = -1, \quad e_{21} = e_{22} = -2, \quad (3)$$

guarantees the existence of stable heteroclinic cycles. An ensemble of 20,000 initial conditions was generated by sampling the uniform distribution on a four-dimensional cube  $-0.5 \leq \text{Re}, \text{Im } z_{1,2} \leq 0.5$  and integrated in time for  $T = 600$ .

Since heteroclinic cycles are attracting all the trajectories in this regime, all solutions spend most of their time near the circle of equilibria. Thus, we expect that the invariant measure for  $z_1$  and  $z_2$  will be concentrated mostly on the circle of equilibria  $z_1 = 0, z_2 = \sqrt{-\mu_2/e_{22}}e^{i\phi}$  with the uniform distribution for the phase,  $\phi$ , on  $[0, \dots, 2\pi]$ .

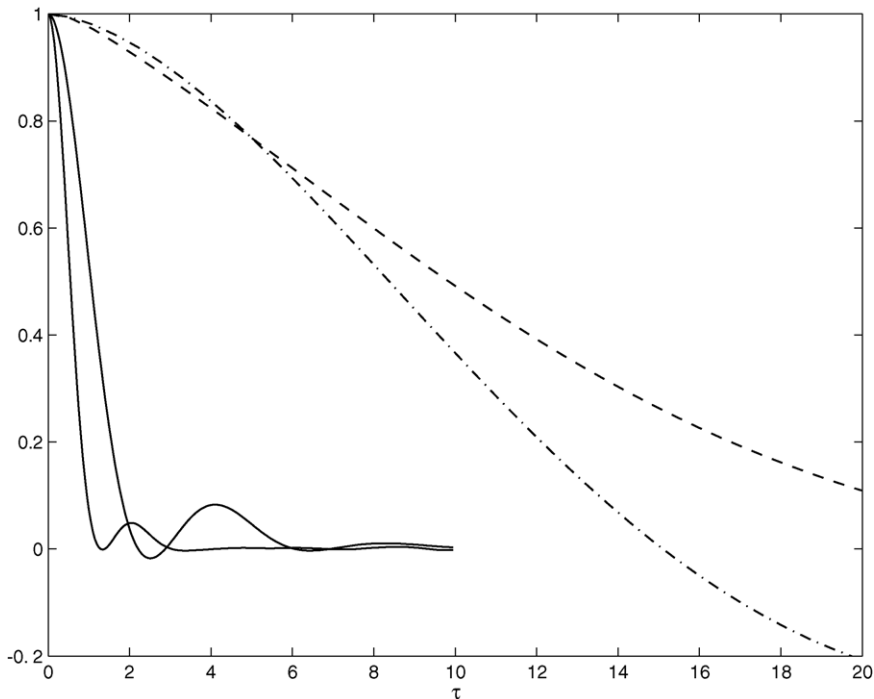


Fig. 7. Direct numerical simulations of the Additive Coupled Model with  $\lambda = 2$ ; normalized correlation functions of  $z_1$  (dashed line) and  $z_2$  (dash-dotted line) and normalized correlation functions of the modes  $u_1$  and  $u_2$  (solid lines).

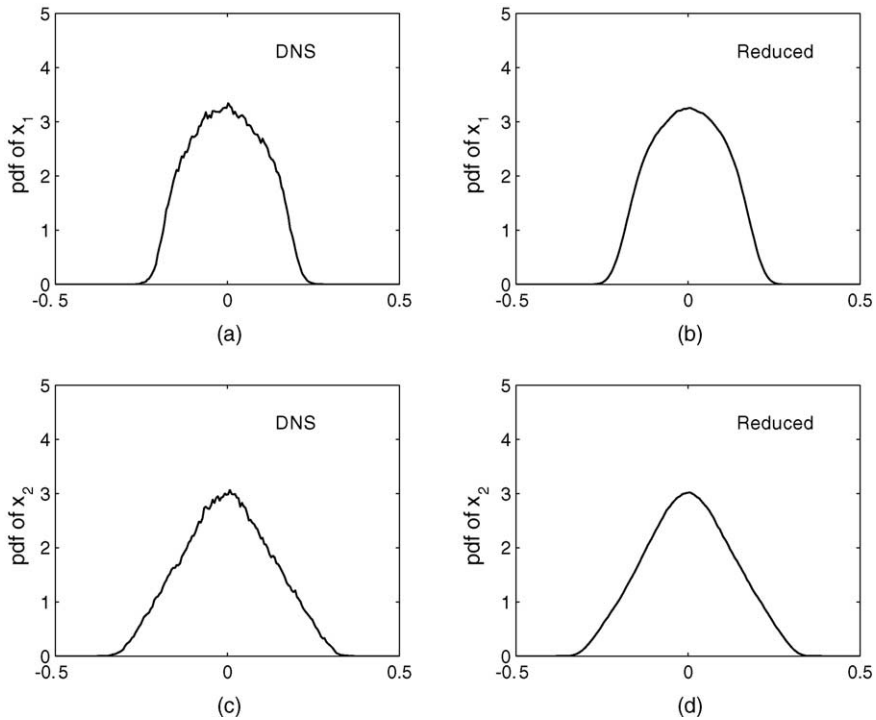


Fig. 8. Additive Model with  $\lambda = 2$ ; marginal PDFs of  $x_1 = \text{Re } z_1$  and  $x_2 = \text{Re } z_2$  for the direct numerical simulations (DNS) of the full equations in (4) and reduced stochastic model in (8).

A small, but finite, probability also exists for the solution to be out of the  $z_1 = 0$  plane with  $z_2$  strictly inside the circle of equilibria. This probability corresponds to the heteroclinic bursts. This is, indeed, the case for long times. Surprisingly, different coherent structures in the Monte-Carlo probability density functions (PDFs) emerge on intermediate time scales; these structures can not be predicted from the long-time properties of the system in (1). This

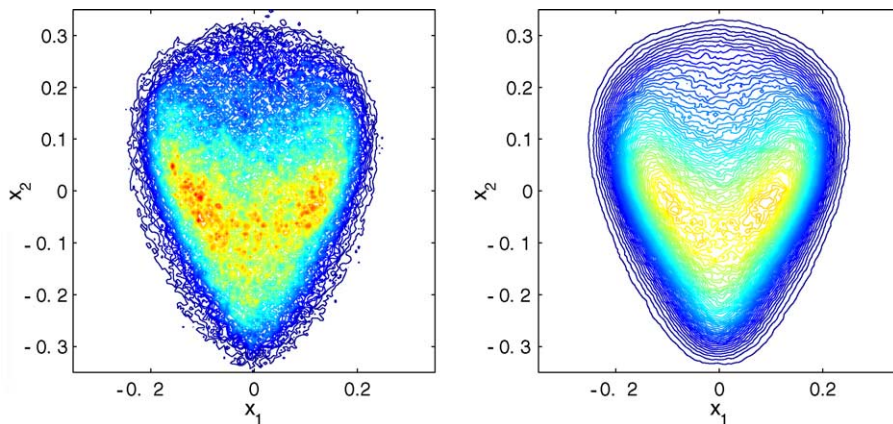


Fig. 9. Additive Model with  $\lambda = 2$ ; joint PDF of the  $x_1, x_2$  computed utilizing bin counting from the DNS of the full model in (4) (left part) and reduced stochastic model in (8) (right part); the figure is color-coded on the interval  $[0, \dots, 13]$  with red color denoting the maximum of the PDF and blue color denoting the minimum value.

is best illustrated by the joint probability distributions of  $z_1$  and  $z_2$ . Utilizing running statistical averages we determine that the simulations reach the expected statistical steady state for times  $t \geq 300$  and the times  $t \in [0, \dots, 300]$  represent the transient state. Figs. 2 and 3 show joint probability distributions of  $\text{Re } z_1, \text{Re } z_2$  and  $\text{Re } z_1, \text{Im } z_2$  for times  $t = 30, 63, 132, 252$ . For times  $t \in [0, \dots, 100]$  prominent structures emerge in both distributions. The heart-like shape with peaks at  $(x_1, x_2) = (\pm 0.1, 0), (0, 0.3)$  is characteristic for the joint PDF  $\text{Re } z_1, \text{Re } z_2$  (top part of Fig. 2). While the second peak,  $(x_1, x_2) = (0, 0.3)$  is related to the heteroclinic connections, the appearance of the peaks  $(x_1, x_2) = (\pm 0.1, 0)$  can not be attributed to the presence of stable heteroclinic cycles. The diamond-like shape in the distribution of  $\text{Re } z_1, \text{Im } z_2$  with large peak at  $(x_1, y_2) = (0, 0)$  also persists for a long time. Toward the end of the transient period,  $t = 252$ , all PDFs converge to a uniform distribution on the circle  $|z_2| = \sqrt{-\mu_2/e_{22}}$  with some residuals of the coherent structures discussed above, and by the end of the transient period all PDFs are in a perfect agreement with the expected result. The appearance of the coherent structures is related to the non-equilibrium properties of the uncoupled model, but below we observe similar shapes for the equilibrium statistics of the coupled systems with 104 degrees of freedom. The initial transient behavior of the system can be understood by analyzing the generic behavior of each individual trajectory. Time series of a single realization on time interval  $[0, \dots, 600]$  are depicted in Fig. 4. During the initial transient  $t \in [0, \dots, 100]$  the trajectory approaches the stable heteroclinic cycle along a modulated periodic motion in  $x_2$  and  $y_2$  variables. This periodic motion is much faster than the irregular spikes in the  $x_1$  and  $y_1$  variables, and it is not surprising that the distribution of  $x_2$  and  $y_2$  is concentrated at zero for short transient times. Marginal PDFs for  $x_1$  and  $x_2$  are depicted in Figs. 5 and 6. Marginal PDFs of  $x_1$  for short times (i.e.  $t = 30, 63$ ) are much broader than the PDFs of  $x_1$  for times corresponding to the heteroclinic regime ( $t = 252$ ). Thus, on average  $x_1$  spends much more time away from zero during the transient regime than during the later equilibrium phase. The situation with  $x_2$  is exactly the opposite. The heteroclinic regime is characterized by  $x_2$  staying away from zero for extended periods of time (see Fig. 1) which is manifested in two peaks in the marginal

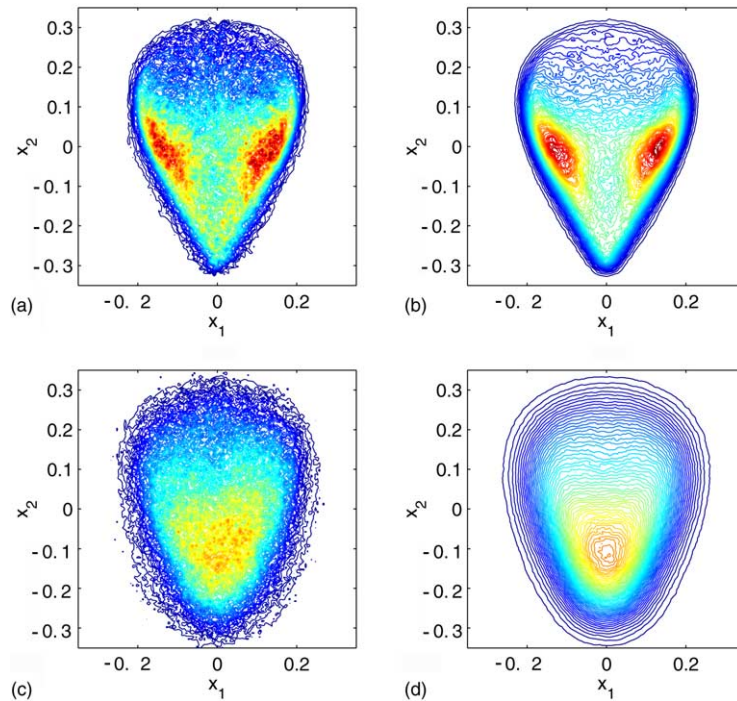


Fig. 10. Additive Model; joint PDF for  $x_1, x_2$ ; (a) full equations in (4) with  $\lambda = 1$ ; (b) reduced model in (8) for  $\lambda = 1$ ; (c) full equations in (4) with  $\lambda = 4$ ; (d) reduced model in (8) for  $\lambda = 4$ ; the figure has the same color-coding as Fig. 9.

PDF of  $x_2$  during the equilibrium heteroclinic phase. On the other hand, during the transient phase,  $x_2$  follows a modulated periodic motion and, thus, crosses zero much more often compared with the equilibrium distribution. The behavior of  $y_1$  is analogous to  $x_1$ , and the behavior of  $y_2$  is analogous to  $x_2$ . The corresponding data for  $y_1$  and  $y_2$  is not presented here for brevity of presentation.

#### 4. Intrinsic stochastic noise versus chaotic dynamics with homoclinic chaos

The systematic mode-reduction strategy developed in [34,35] has two steps. The first step consists of replacing the original deterministic model by an intermediate stochastic system where the deterministic self-interactions of the fast unresolved variables are replaced by stochastic terms. The stochastic mode reduction is the second step where all the fast unresolved variables are eliminated and closed-form stochastic differential equations for the reduced variables are derived. In this section we introduce two types of coupled models: “additive noise” and “multiplicative noise” to systematically examine the interaction between the internal chaotic dynamics of the reduced variables and the intrinsic stochasticity of the heat bath and to test the overall performance of the mode reduction strategy in several different regimes. When the stochastic mode-reduction strategy is successful, we have a simplified low-dimensional stochastic model for the interactions. For these purposes the first step of the mode-reduction strategy will be addressed here only briefly. For detailed discussion of this procedure and various approaches for determining the stochastic parameters see [36,37]. The equations in (2) with  $\Lambda = 50$  are utilized as a heat bath in the examples below.

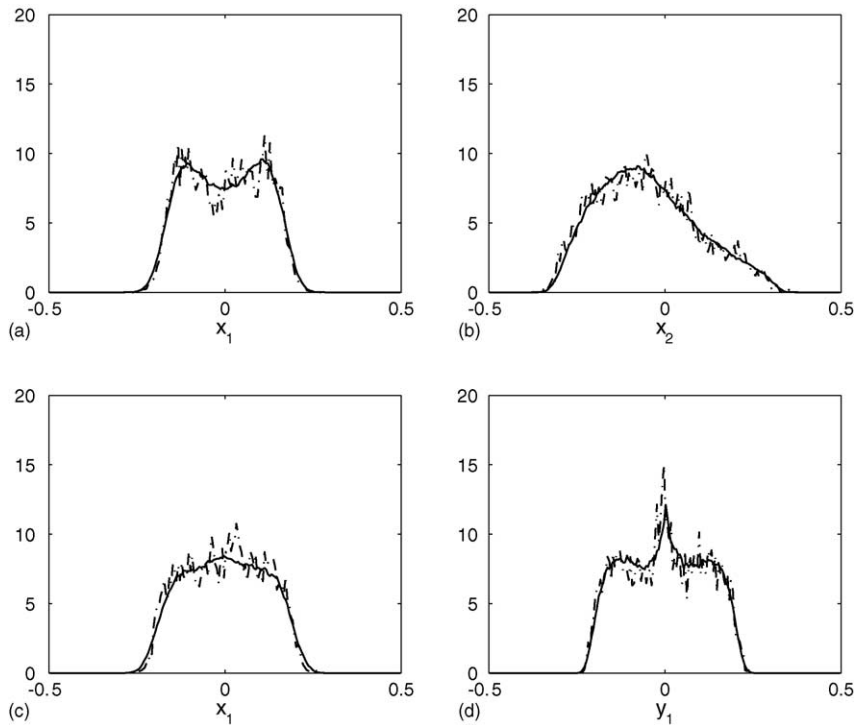


Fig. 11. Additive Model with  $\lambda = 2$ ; conditional PDFs (the same as cross-sections of joint PDFs) of the slow variables; solid line – reduced model in (8); dotted line – DNS of the full system in (4); (a) PDF of  $x_1$  conditional  $x_2 = 0$ ; (b) PDF of  $x_2$  conditional  $x_1 = 0$ ; (c) PDF of  $x_1$  conditional  $y_2 = 0$ ; (d) PDF of  $y_1$  conditional  $x_1 = 0$ .

Direct numerical simulations of the coupled systems are performed utilizing a standard pseudo-spectral method in space and fourth order Runge–Kutta stepping in time. Unless otherwise specified the statistics are computed utilizing time-averaging from a single realization. See [36,37] for a detailed discussion of this procedure.

4.1. Additive coupling

The first example considered here is the deterministic “additive” model with 104 degrees of freedom ( $1 \leq k \leq \Lambda$ ) given by

$$\begin{aligned} \dot{z}_1 &= z_1^* z_2 + (\mu_1 + e_{11}|z_1|^2 + e_{12}|z_2|^2)z_1 + \lambda (b^{x_1|u_1} + ib^{y_1|u_1}) v_1 w_1, \\ \dot{z}_2 &= -z_1^2 + (\mu_2 + e_{21}|z_1|^2 + e_{22}|z_2|^2)z_2 + \lambda(b^{x_2|u_2} + ib^{y_2|u_2})v_2 w_2, \\ \dot{u}_1 &= \{\text{TBH}\} + \lambda(b^{v_1|x_1 w_1} x_1 w_1 + b^{v_1|y_1 w_1} y_1 w_1) + i\lambda(b^{w_1|x_1 v_1} x_1 v_1 + b^{w_1|y_1 v_1} y_1 v_1), \\ \dot{u}_2 &= \{\text{TBH}\} + \lambda(b^{v_2|x_2 w_2} x_2 w_2 + b^{v_2|y_2 w_2} y_2 w_2) + i\lambda(b^{w_2|x_2 v_2} x_2 v_2 + b^{w_2|y_2 v_2} y_2 v_2), \\ \dot{u}_k &= \{\text{TBH}\} = -\frac{ik}{2} \sum_{p+q+k=0} \hat{u}_p^* \hat{u}_q^*, \quad 2 < k \leq \Lambda, \end{aligned} \tag{4}$$

where {TBH} denotes the Truncated Burgers–Hopf terms introduced in (2). The coupling is selected in such a way that the mode  $z_1$  is coupled only to  $u_1$  and mode  $z_2$  is coupled to  $u_2$ ; the interactions considered in (4) produce

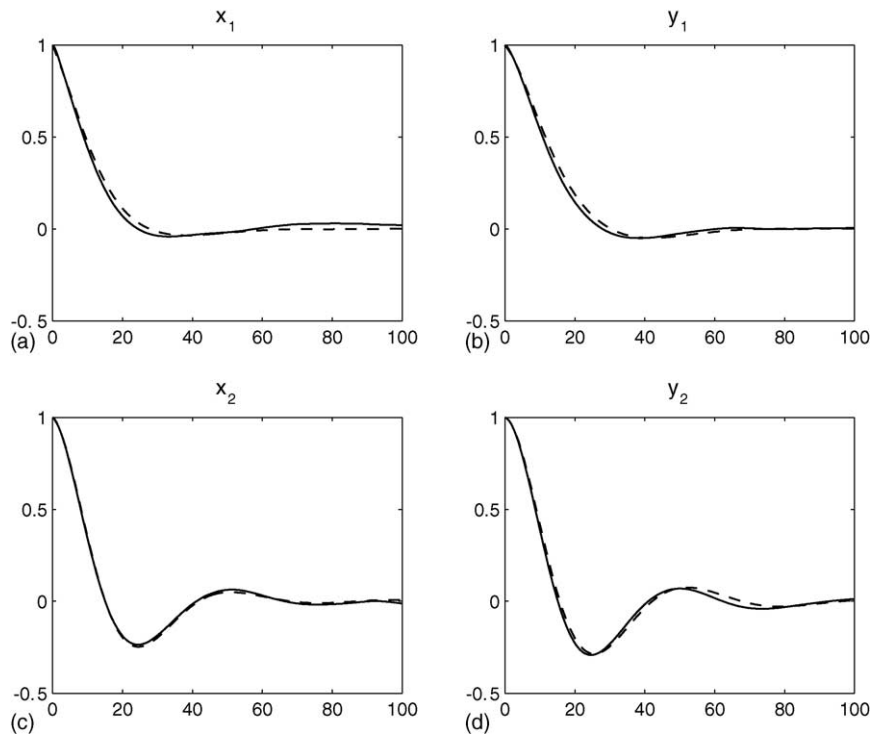


Fig. 12. Additive Model with  $\lambda = 2$ ; normalized correlation functions for  $x_{1,2}$  and  $y_{1,2}$ ; solid lines – direct numerical simulations of the full equations in (4); dashed lines – reduced stochastic model in (8).

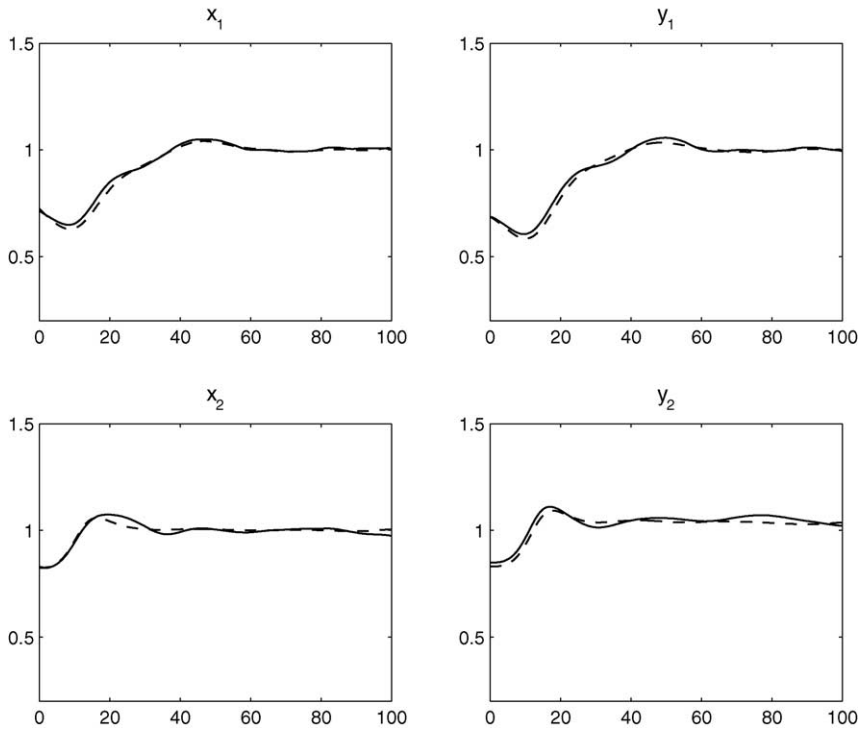


Fig. 13. Additive Model with  $\lambda = 2$ ; normalized correlation of energy for  $x_{1,2}$  and  $y_{1,2}$ ; solid lines – direct numerical simulations of the full equations in (4); dashed lines – reduced stochastic model in (8).

corrections of the Ornstein–Uhlenbeck type for the reduced variables. A particular simple choice of interaction coefficients is presented in Table 1 and the parameter  $\lambda$  is introduced explicitly to control the strength of interaction between  $z_1, z_2$  and the unresolved modes,  $u_k$ .

Equations in (4) with  $\lambda = 2$  were integrated for  $T = 100,000$  with parameters in the equations for  $z_1, z_2$  presented previously in (3). Comparison of correlation functions for  $z_1$  and  $z_2$  with correlation functions for  $u_{1,2}$  is presented in Fig. 7. Even with coupling, the heat bath of 100 modes has essentially equipartition of energy with variance  $\text{Var}\{\text{Re}, \text{Im } u_k\} \approx 0.012$  which according to Table 2 is comparable to the variance of  $z_1, z_2$ . Although average energy of the  $z_1, z_2$  variables is comparable with the average energy in the bath modes,  $u_k$ , the modes  $z_1$  and  $z_2$  have much longer correlations and, thus, are natural slow variables of the system. Moreover, the cross-correlations between all possible combinations of the real and imaginary parts of  $z_1$  and  $z_2$  are two orders of magnitude smaller than their variances. Thus,  $(x_1, y_1) = (\text{Re } z_1, \text{Im } z_1)$  and  $(x_2, y_2) = (\text{Re } z_2, \text{Im } z_2)$  are also natural empirical orthogonal functions of the systems in (4) with diagonal covariance matrix.

Table 3

Interaction coefficients for multiplicative models of Type I in (12) (first and second rows) and Type II in (15) (third and fourth rows)

|                           |                           |                       |
|---------------------------|---------------------------|-----------------------|
| $b^{x_1 y_1 v_1} = -0.75$ | $b^{y_1 x_1 v_1} = -0.25$ | $b^{v_1 x_1 y_1} = 1$ |
| $b^{x_2 y_2 v_2} = -0.75$ | $b^{y_2 x_2 v_2} = -0.25$ | $b^{v_2 x_2 y_2} = 1$ |
| $b^{x_1 y_2 v_1} = -0.75$ | $b^{y_2 x_1 v_1} = -0.25$ | $b^{v_1 x_1 y_2} = 1$ |
| $b^{x_2 y_1 v_2} = -0.75$ | $b^{y_1 x_2 v_2} = -0.25$ | $b^{v_2 x_2 y_1} = 1$ |

Table 4

Multiplicative Model of Type I with  $\lambda = 1$ ; one-point statistics of the slow variables computed from the DNS of the full system in (12) and reduced model in (13)

|                  | $x_1$   | $y_1$    | $x_2$    | $y_2$     |
|------------------|---------|----------|----------|-----------|
| Mean DNS         | 0.00058 | −0.00162 | −0.00624 | −0.0006   |
| Mean reduced     | 0.00061 | 0.00012  | −0.01191 | −0.000061 |
| Var DNS          | 0.01072 | 0.01064  | 0.01529  | 0.01754   |
| Var reduced      | 0.01075 | 0.01105  | 0.01369  | 0.01994   |
| Skewness DNS     | 0.0017  | 0.0124   | −0.0671  | −0.0069   |
| Skewness reduced | −0.0059 | −0.0048  | 0.0055   | −0.0012   |
| Flatness DNS     | 1.98106 | 2.01715  | 2.66309  | 2.51052   |
| Flatness reduced | 1.94827 | 1.91961  | 2.71078  | 2.21453   |

In the first step of the stochastic modeling strategy, the deterministic self-interactions of the bath modes,  $u_k$ , in the equations for  $u_1$  and  $u_2$  are approximated by an Ornstein–Uhlenbeck process, i.e.,

$$-\frac{ik}{2} \sum_{p+q+k=0} \hat{u}_p^* \hat{u}_q^* \approx -\gamma_k u_k + \sigma_k \dot{W}_k, \tag{5}$$

$$\frac{\sigma_k^2}{\gamma_k} = \text{Var}\{u_k\}. \tag{6}$$

With the approximation in (5) the additive coupled system in (4) becomes, essentially, an eight-dimensional stochastic differential equation, since the bath modes  $u_1$  and  $u_2$  decouple from the rest of the fast modes. Parameters

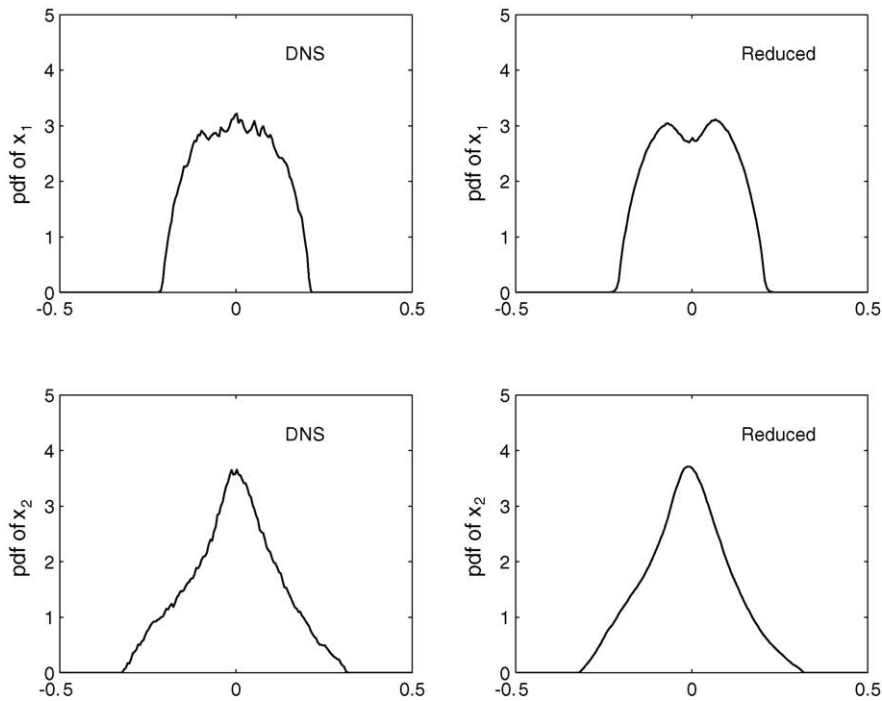


Fig. 14. Multiplicative Model; marginal PDFs of  $x_1 = \text{Re } z_1$  and  $x_2 = \text{Re } z_2$  for the direct numerical simulations (DNS) of the full equations in (12) and reduced stochastic model in (13).

$\gamma_k$  are determined crudely as the inverse of the area under the graph of the modulus of the correlation function for  $u_k$  (see [36,37]). As mentioned earlier the heat bath,  $u_k$ , achieves an equipartition of energy with  $\langle u_k^2 \rangle \approx 0.025$  and parameters  $\sigma_k$  are determined from the equation in (6). Estimates for these parameters are

$$\gamma_1 = 0.7139, \quad \gamma_2 = 1.4083, \quad \sigma_1 = 0.1371, \quad \sigma_2 = 0.1929. \tag{7}$$

Unlike for the conservative “additive” systems reported in [36], in this case the stochastic mode-reduction procedure is insensitive to small changes in  $\gamma_k$  and  $\sigma_k$ . Small fluctuations in these parameters have essentially no effect on the statistical behavior of the reduced system and we expect that the stochastic mode-elimination procedure applied to any system with internal chaotic dynamics in the reduced variables will produce very robust results which do not require any fine-tuning of the stochastic parameters  $\gamma_k$  and  $\sigma_k$ . Applying the stochastic mode-reduction step developed in [35,36] to the stochastic equations for  $z_{1,2}$  and  $u_{1,2}$  we obtain the reduced model for the slow variables  $z_1$  and  $z_2$  (written through the real and imaginary parts for explicit representation)

$$\begin{aligned} \begin{pmatrix} x_1 \\ y_1 \end{pmatrix}' &= \begin{pmatrix} x_1 x_2 + y_1 y_2 + x_1(\mu_1 + e_{11}r_1^2 + e_{12}r_2^2) \\ x_1 y_2 - y_1 x_2 + y_1(\mu_1 + e_{11}r_1^2 + e_{12}r_2^2) \end{pmatrix} - A_1(x_1, y_1)^T + \Sigma_1(W_1, W_2)^T, \\ \begin{pmatrix} x_2 \\ y_2 \end{pmatrix}' &= \begin{pmatrix} -(x_1^2 - y_1^2) + x_2(\mu_2 + e_{21}r_1^2 + e_{22}r_2^2) \\ -2x_1 y_1 + y_2(\mu_2 + e_{21}r_1^2 + e_{22}r_2^2) \end{pmatrix} - A_2(x_2, y_2)^T + \Sigma_2(W_3, W_4)^T, \end{aligned} \tag{8}$$

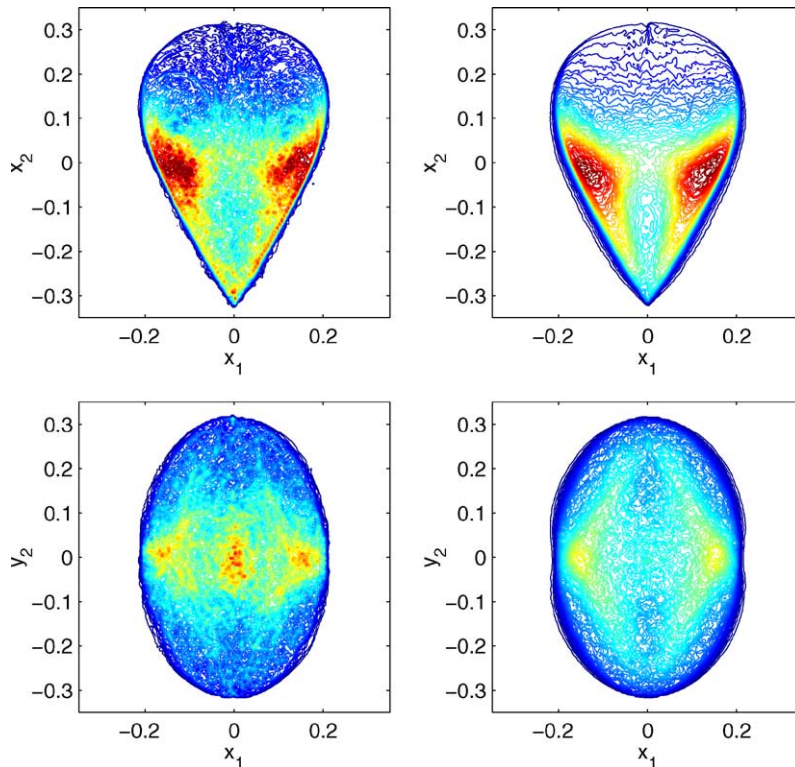


Fig. 15. Multiplicative Model; joint PDF of the  $x_1, x_2$  computed utilizing bin counting from the DNS of the full model in (12) (left part) and reduced stochastic model in (13) (right part); the Figure is color-coded on the interval  $[0, \dots, 13]$  with red color denoting the maximum of the PDF and blue color denoting the minimum value.

where  $r_k^2 = |z_k|^2 = x_k^2 + y_k^2$ ,  $W_j$  are independent Wiener processes and constant matrices  $A_{1,2}$  and  $\Sigma_{1,2}$  are expressed explicitly through the interaction coefficients  $b^{i,j}$  and parameters  $\gamma_k$  and  $\sigma_k$ :

$$A_1 = -\frac{\lambda^2 \sigma_1^2}{4\gamma_1^2} \begin{pmatrix} b^{x_1|u_1}(b^{v_1|x_1 w_1} + b^{w_1|x_1 v_1}) & b^{x_1|u_1}(b^{v_1|y_1 w_1} + b^{w_1|y_1 v_1}) \\ b^{y_1|u_1}(b^{v_1|x_1 w_1} + b^{w_1|x_1 v_1}) & b^{y_1|u_1}(b^{v_1|y_1 w_1} + b^{w_1|y_1 v_1}) \end{pmatrix}, \quad \Sigma_1^2 = \frac{\sigma_1^2}{\gamma_1} A_1,$$

$$A_2 = -\frac{\lambda^2 \sigma_2^2}{4\gamma_2^2} \begin{pmatrix} b^{x_2|u_2}(b^{v_2|x_2 w_2} + b^{w_2|x_2 v_2}) & b^{x_2|u_2}(b^{v_2|y_2 w_2} + b^{w_2|y_2 v_2}) \\ b^{y_2|u_2}(b^{v_2|x_2 w_2} + b^{w_2|x_2 v_2}) & b^{y_2|u_2}(b^{v_2|y_2 w_2} + b^{w_2|y_2 v_2}) \end{pmatrix}, \quad \Sigma_2^2 = \frac{\sigma_2^2}{\gamma_2} A_2.$$

Substituting the interaction coefficients from Table 1 and computing  $\sqrt{A_1}$  and  $\sqrt{A_2}$  numerically we obtain

$$A_1 = \frac{\lambda^2 \sigma_1^2}{4\gamma_1^2} \begin{pmatrix} 1 & -0.7 \\ -0.7 & 0.49 \end{pmatrix}, \quad \Sigma_1 = \frac{\lambda \sigma_1^2}{2\gamma_1 \sqrt{\gamma_1}} \begin{pmatrix} 0.8192 & -0.5735 \\ -0.5735 & 0.4014 \end{pmatrix}, \tag{9}$$

$$A_2 = \frac{\lambda^2 \sigma_2^2}{4\gamma_2^2} \begin{pmatrix} 1 & -0.55 \\ -0.55 & 0.3025 \end{pmatrix}, \quad \Sigma_2 = \frac{\lambda \sigma_2^2}{2\gamma_2 \sqrt{\gamma_2}} \begin{pmatrix} 0.8762 & -0.4819 \\ -0.4819 & 0.2651 \end{pmatrix}. \tag{10}$$

The reduced equations in (8) with  $\lambda = 2$  and the estimates for  $\gamma_k$  and  $\sigma_k$  from (7) were integrated for  $T = 1,000,000$  using the second order Runge–Kutta method for the deterministic terms and a straightforward stochastic Euler

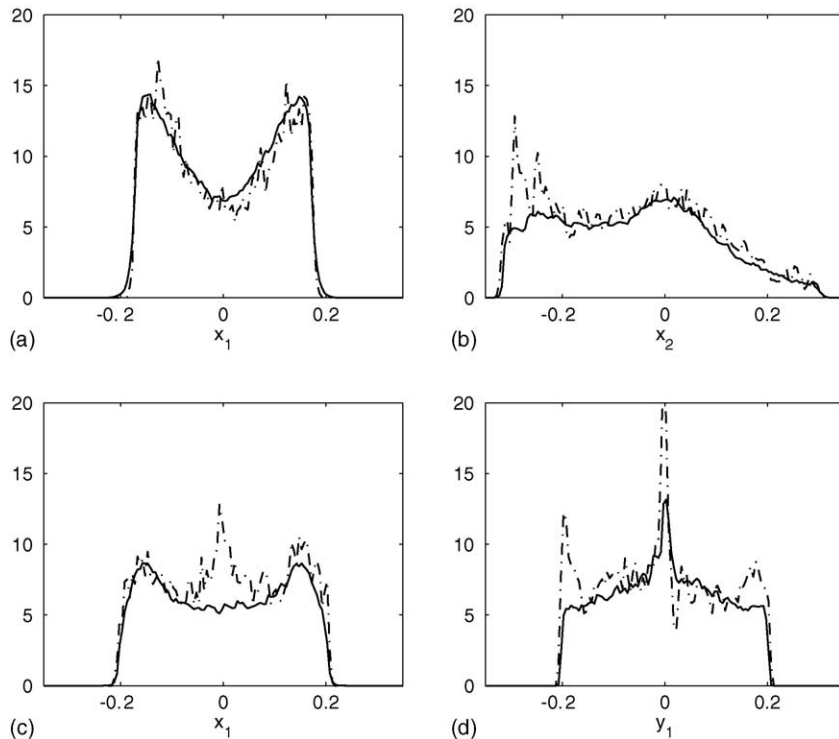


Fig. 16. Multiplicative Model; conditional PDFs (the same as cross-sections of joint PDFs) of the slow variables; solid line – reduced model in (13); dotted line – DNS of the full system in (12); (a) PDF of  $x_1$  conditional  $x_2 = 0$ ; (b) PDF of  $x_2$  conditional  $x_1 = 0$ ; (c) PDF of  $x_1$  conditional  $y_2 = 0$ ; (d) PDF of  $y_1$  conditional  $x_1 = 0$ .

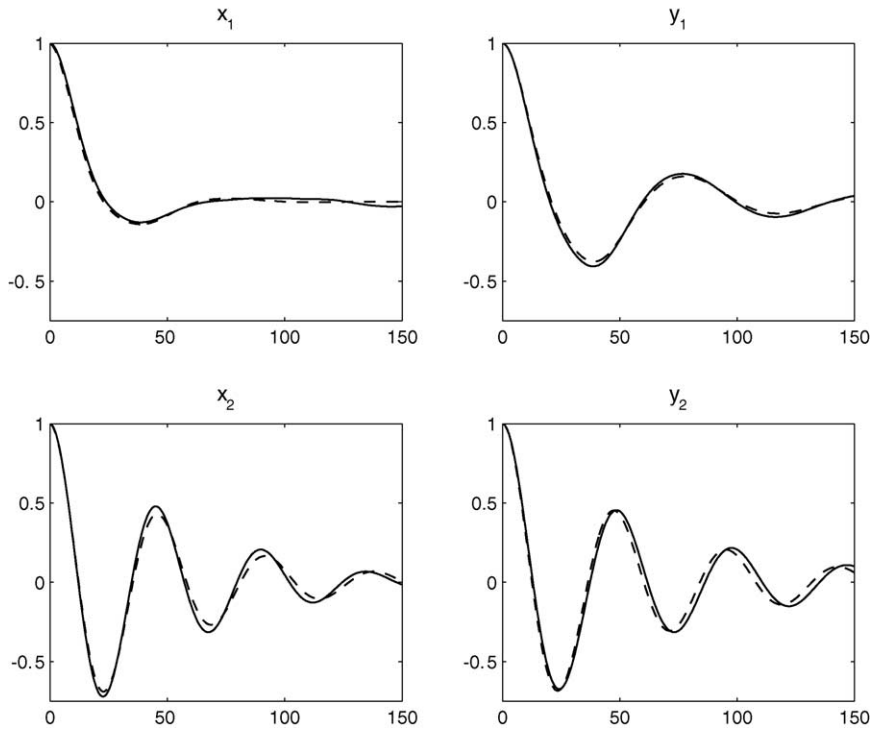


Fig. 17. Multiplicative Model; normalized correlation functions for  $x_{1,2}$  and  $y_{1,2}$ ; solid lines – direct numerical simulations of the full equations in (12); dashed lines – reduced stochastic model in (13).

method (see [28]) to discretize the white noise terms. All statistics were computed as time averages from a single realization.

Comparison of the PDFs of the slow variables  $x_1 = \text{Re } z_1$  and  $x_2 = \text{Re } z_2$  from the direct numerical simulations (DNS) of the full equations with 104 degrees of freedom in (4) and four-dimensional reduced stochastic model in (8) is depicted in Fig. 8. Results for the PDFs of  $y_1 = \text{Im } z_1$  and  $y_2 = \text{Im } z_2$  are qualitatively similar and not presented here. Comparison of the low order statistics for the slow variables is presented in Table 2. In addition to obvious comparison of these statistical quantities we also performed a severe test for the one-point statistics where we compared the joint PDFs of the slow variables. Fig. 9 shows comparison of the joint PDF of  $x_1, x_2$  computed from the simulations of the full system with 104 degrees of freedom in (4) and reduced equations in (8). Comparison of cross-sections of selected joint PDFs is depicted in Fig. 11. The stochastic mode-reduction strategy reproduces the statistics of the full system with remarkable accuracy, including the complicated structure and magnitude of the peaks in the joint PDFs of the slow variables. Next, we present comparison of the two-point statistics for the

Table 5

Comparison of Multiplicative Models of Type I and II with  $\lambda = 0.25$ ; one-point statistics of the slow variables computed from the DNS of the full systems in (12) (Type I) and in (15) (Type II)

|                   | $x_1$   | $y_1$   | $x_2$   | $y_2$   |
|-------------------|---------|---------|---------|---------|
| Var, Type I       | 0.00903 | 0.00902 | 0.01573 | 0.02943 |
| Flatness, Type I  | 2.25    | 2.26    | 2.91    | 1.95    |
| Var, Type II      | 0.00897 | 0.0089  | 0.0291  | 0.0166  |
| Flatness, Type II | 2.72    | 2.72    | 1.97    | 2.68    |

slow variables. In addition to the usual test for the correlation functions depicted in Fig. 12, we also compute the normalized correlation of energy

$$K_q(s) = \frac{\langle q^2(s)q^2(t+s) \rangle}{\langle q^2 \rangle^2 + 2\langle q(s)q(t+s) \rangle^2}. \quad (11)$$

This quantity measures the correlation in time of the energy,  $q^2(t)$ , in the mode: it is appropriately normalized so that  $K(t) = 1$  for all time for a Gaussian  $q$  [36,37]. The two-point statistics of the slow variables, including the oscillations in the correlation functions and non-Gaussian behavior is captured extremely well by the reduced four-dimensional stochastic model. Overall, there is a remarkable agreement between the statistical behavior of the slow variables in the deterministic coupled system and in the reduced low-dimensional model. Moreover, we have performed a systematic study of the model in (4) by varying the strength of coupling  $\lambda = 0.25, \dots, 7$ . Although, this parameter enters as  $\lambda^2$  in the time-scale of the slow variables in the reduced equation (see (9) and (10)), for the regime  $\lambda = 2$  the strength of the noise terms is roughly comparable with the cubic nonlinear terms and much smaller than the quadratic terms in the reduced equation in (8). Of course, the non-dimensional form of the reduced equations is needed to correctly assess the relative strength of various terms in the equation which confirm the above statement; derivation of the non-dimensional form of the reduced model is presented in Appendix A. For other references related to this issue see also the detailed discussion of the non-dimensionalization in [36]. The estimates for the non-dimensionalization are not precise and serve only as guidelines for understanding the relative strength of the noise. It is evident from the formulas for  $A_{1,2}$  and  $\Sigma_{1,2}$  in (9) and (10) that smaller values of  $\lambda$  correspond to cases with very weak noise. We obtained an extremely good agreement between the full equations in (4) and the reduced model in (8) for the range of the coupling strength  $\lambda = 0.25, \dots, 5$ . For larger values of  $\lambda$  discrepancies

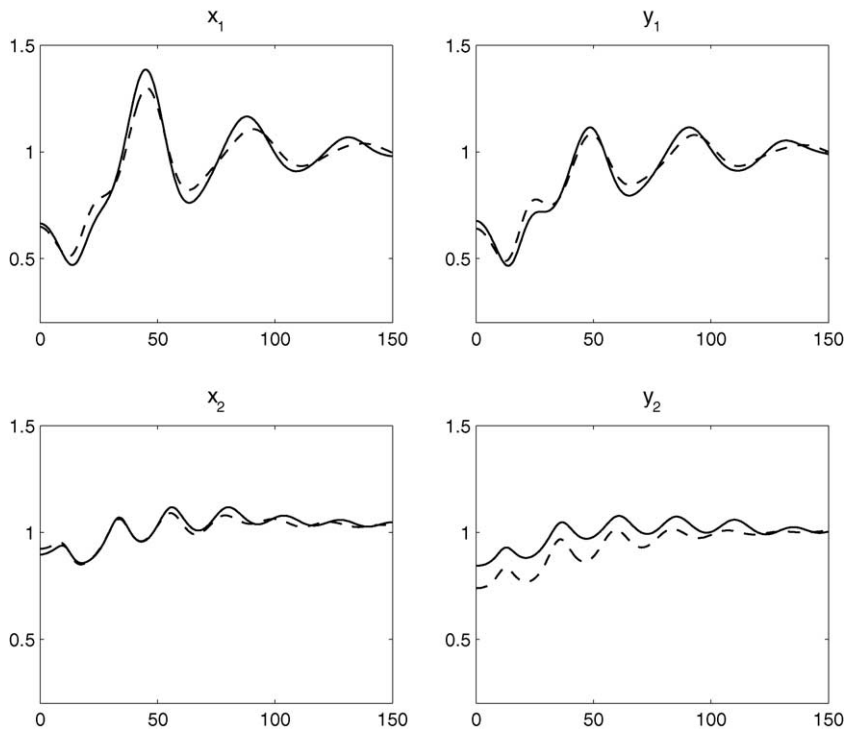


Fig. 18. Multiplicative Model; normalized correlation of energy for  $x_{1,2}$  and  $y_{1,2}$ ; solid lines – direct numerical simulations of the full equations in (12); dashed lines – reduced stochastic model in (13).

begin to appear first in the two-point statistics and then in the PDFs of the slow variables. To illustrate the drastic effect the coupling has on the statistics of the slow variables we present the joint PDF of  $x_1, x_2$  for regimes  $\lambda = 1, 4$  in Fig. 10. This PDF has two disjoint peaks for  $\lambda = 1$  with the overall structure closely resembling the statistics on intermediate times of the Monte-Carlo simulation of the uncoupled model described in Section 3 (see Fig. 2). Under the stronger coupling (Fig. 9) the two peaks merge and form a complicated “boomerang” shape. Finally, for  $\lambda = 4$  only one large peak remains in the joint PDF of  $x_1, x_2$ . Other statistics of the slow variables also undergo nontrivial transitions as the strength of the coupling is increased. We would like to emphasize that the reduced model captures these transitions in all statistical quantities extremely well and these results are not presented here only for brevity of presentation.

#### 4.2. Multiplicative coupling

In the second example, the multiplicative type of coupling is examined more closely and the importance of the noise is demonstrated on cases with very weak coupling. The multiplicative model is constructed in a manner similar to the additive example in Section 4.1, except the interactions are chosen in such a way, that they produce nonlinear corrections and multiplicative noises in the reduced model [34–37]. Written through complex notation the multiplicative model with 104 degrees of freedom is given by

$$\begin{aligned} \dot{z}_1 &= z_1^* z_2 + (\mu_1 + e_{11}|z_1|^2 + e_{12}|z_2|^2)z_1 + \lambda v_1 (b^{x_1|y_1} v_1 y_1 + i b^{y_1|x_1} v_1 x_1), \\ \dot{z}_2 &= -z_1^2 + (\mu_2 + e_{21}|z_1|^2 + e_{22}|z_2|^2)z_2 + \lambda v_2 (b^{x_2|y_2} v_2 y_2 + i b^{y_2|x_2} v_2 x_2), \\ \dot{u}_k &= -\frac{ik}{2} \sum_{p+q+k=0} \hat{u}_p^* \hat{u}_q^* + \lambda \delta_{1,k} b^{v_1|x_1} v_1 x_1 y_1 + \lambda \delta_{2,k} b^{v_2|x_2} v_2 x_2 y_2. \end{aligned} \tag{12}$$

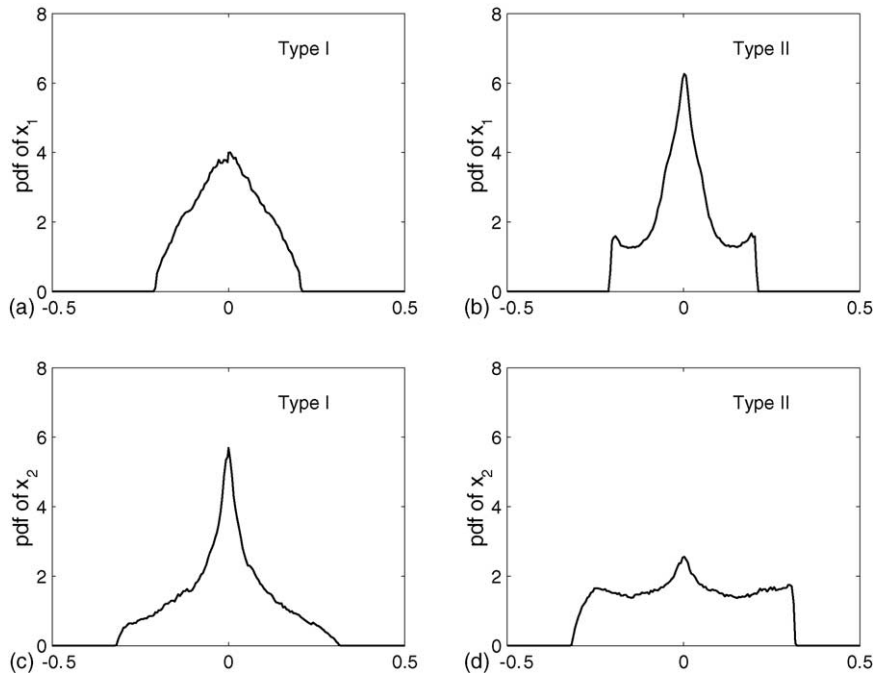


Fig. 19. Comparison of Multiplicative Models of Type I and II with  $\lambda = 0.25$ ; marginal PDFs of  $x_1$  and  $x_2$ ; left column – simulations of the multiplicative model of Type I in (12); right column – simulations of the multiplicative model of Type II in (15).

Thus, in this example  $x_1$  and  $y_1$  are coupled only to  $v_1 = \text{Re } u_1$  and  $x_2$  and  $y_2$  are coupled only to  $v_2 = \text{Re } u_2$ . We will refer to this model as the multiplicative system of Type I. This model is considered with the same parameter values in (3) and interaction coefficients presented in Table 3. For a wide range of coupling strengths,  $\lambda$ , the average energy distribution and difference in correlation times is qualitatively similar to the additive case discussed in Section 4.1 and modes  $z_1$  and  $z_2$  play the role of natural slow variables of the system in (12) with diagonal covariance matrix. The stochastic mode-reduction procedure is carried out in a similar manner. With the approximation in (5) we apply Theorem 4.3 from [35] to the six-dimensional system of  $z_1, z_2, \text{Re } u_1$  and  $\text{Re } u_2$  and obtain the reduced stochastic model for the slow variables alone

$$\begin{aligned}
 \dot{x}_1 &= x_1 x_2 + y_1 y_2 + x_1(\mu_1 + e_{11}r_1^2 + e_{12}r_2^2) + N_1 y_1^2 x_1 + A_1 x_1 + S_1 y_1 \dot{W}_1, \\
 \dot{y}_1 &= x_1 y_2 - y_1 x_2 + y_1(\mu_1 + e_{11}r_1^2 + e_{12}r_2^2) + N_2 y_1 x_1^2 + A_1 y_1 + S_2 x_1 \dot{W}_1, \\
 \dot{x}_2 &= -(x_1^2 - y_1^2) + x_2(\mu_2 + e_{21}r_1^2 + e_{22}r_2^2) + N_3 y_2^2 x_2 + A_2 x_2 + S_3 y_2 \dot{W}_2, \\
 \dot{y}_2 &= -2x_1 y_1 + y_2(\mu_2 + e_{21}r_1^2 + e_{22}r_2^2) + N_4 y_2 x_2^2 + A_2 y_2 + S_4 x_2 \dot{W}_2,
 \end{aligned}
 \tag{13}$$

where

$$N_1 = \lambda^2 \frac{b^{x_1|y_1 v_1} b^{v_1|x_1 y_1}}{\gamma_1} = -0.75 \frac{\lambda^2}{\gamma_1}, \quad N_2 = \lambda^2 \frac{b^{y_1|x_1 v_1} b^{v_1|x_1 y_1}}{\gamma_1} = -0.25 \frac{\lambda^2}{\gamma_1},$$

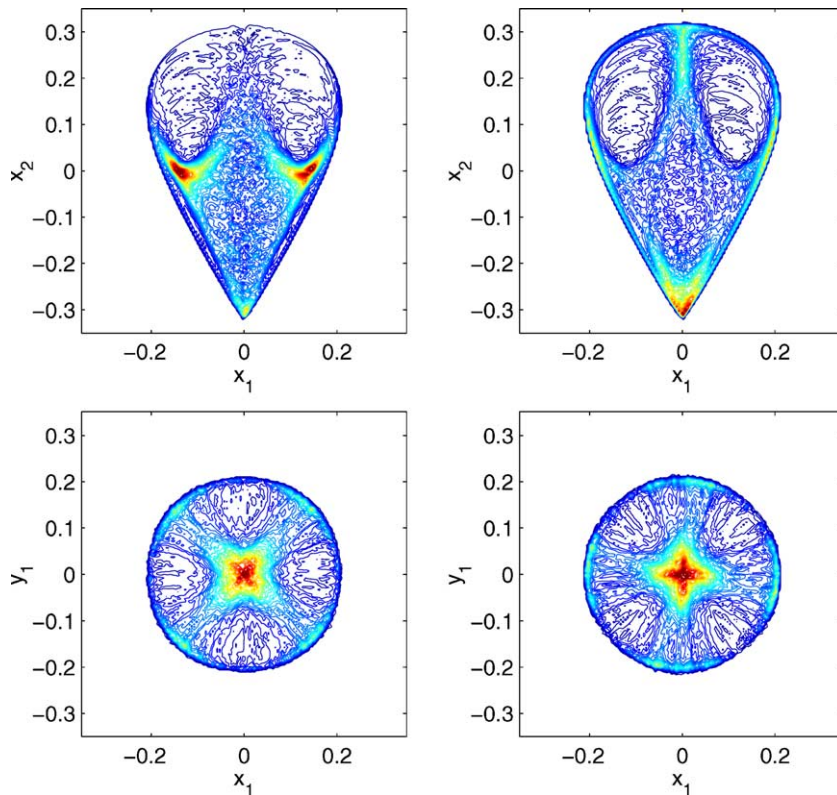


Fig. 20. Comparison of Multiplicative Models of Type I and II with  $\lambda = 0.25$ ; joint PDFs of  $x_1, x_2$  and  $x_1, y_1$ ; left column – simulations of the multiplicative model of Type I in (12); right column – simulations of the multiplicative model of Type II in (15).

$$\begin{aligned}
 N_3 &= \lambda^2 \frac{b^{x_2|y_2 v_2} b^{v_2|x_2 y_2}}{\gamma_2} = -0.75 \frac{\lambda^2}{\gamma_2}, & N_4 &= \lambda^2 \frac{b^{y_2|x_2 v_2} b^{v_2|x_2 y_2}}{\gamma_2} = -0.25 \frac{\lambda^2}{\gamma_2}, \\
 S_1 &= \frac{\lambda \sigma_1}{\gamma_1} b^{x_1|y_1 v_1} = -0.75 \frac{\lambda \sigma_1}{\gamma_1}, & S_2 &= \frac{\lambda \sigma_1}{\gamma_1} b^{y_1|x_1 v_1} = -0.25 \frac{\lambda \sigma_1}{\gamma_1}, \\
 S_3 &= \frac{\lambda \sigma_2}{\gamma_2} b^{x_2|y_2 v_2} = -0.75 \frac{\lambda \sigma_2}{\gamma_2}, & S_4 &= \frac{\lambda \sigma_2}{\gamma_2} b^{y_2|x_2 v_2} = -0.25 \frac{\lambda \sigma_2}{\gamma_2}, \\
 A_1 &= \lambda^2 \frac{\sigma_1^2}{\gamma_1^2} b^{x_1|y_1 v_1} b^{y_1|x_1 v_1} = 0.1875 \frac{\lambda^2 \sigma_1^2}{\gamma_1^2}, & A_2 &= \lambda^2 \frac{\sigma_2^2}{\gamma_2^2} b^{x_2|y_2 v_2} b^{y_2|x_2 v_2} = 0.1875 \frac{\lambda^2 \sigma_2^2}{\gamma_2^2}.
 \end{aligned}$$

In (13) and all equations below, the multiplicative noises are written in the Itô sense [18]. It is difficult to access the exact strength of the noise in a multiplicative model; the non-dimensionalization for (13) presented in Appendix A suggests that regime with  $\lambda = 1$  has multiplicative noises which are comparable with the cubic terms in (13), but smaller in magnitude than the quadratic terms. The system in (12) with  $\lambda = 1$  was integrated for  $T = 100,000$  and statistics of the slow variables,  $z_{1,2}$ , and the heat bath were computed utilizing time-averaging from a single realization. The heat bath,  $u_k$ , is roughly equipartitioned with mean zero and  $\langle v_k^2 \rangle \approx \langle w_k^2 \rangle \approx 0.011$ . Estimates for the decay of correlations,  $\gamma_k$ , and magnitude of the noise,  $\sigma_k$ , in the approximation in (5) are computed in the same manner as before; they are

$$\gamma_1 = 0.613, \quad \gamma_2 = 1.3643, \quad \sigma_1 = 0.117, \quad \sigma_2 = 0.1745. \tag{14}$$

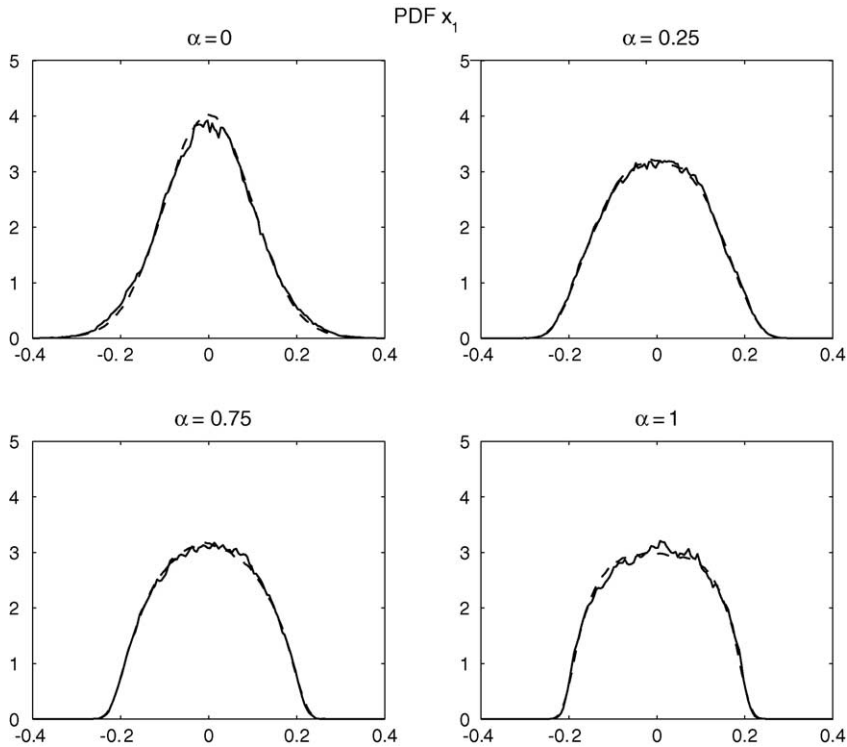


Fig. 21. Marginal PDF of  $x_1$ ; bifurcation with respect to the strength of the nonlinearity in the coupled Additive Model; solid line – full coupled system; dashed – reduced model; two lines overlap on most of the graphs.

The structure of the stochastic terms is entirely different from the additive model considered in Section 4.1. In addition to the multiplicative noise, nonlinear correction also arise that play the role of nonlinear damping which balances the noise. The non-dimensional balance of terms is also very different compared to the additive model discussed above.

Detailed comparison of the one-point statistics, including the selected joint PDFs is presented in Table 4 and Figs. 14–16. This regime does not correspond to a weak noise limit and we observe some minor discrepancies in the joint PDFs of the slow variables. The rest of the statistical quantities computed from the reduced model in (13) are in very good agreement with the direct numerical simulations of the full equations in (12). Comparison of the two-point statistics is depicted in Figs. 17 and 18. The reduced model captures the non-trivial oscillatory structure of correlations and non-Gaussian nature of the process extremely well. Non-Gaussian behavior of solutions is manifested more strongly for the multiplicative model than for the additive case from Section 4.1 (cf. Figs. 13 and 18). Multiplicative noises and nonlinear corrections are essential for the correct reproduction of this behavior in any reduced model and can not be reproduced by a linear stochastic model of the Ornstein–Uhlenbeck type.

4.2.1. Influence of intrinsic stochastic noise

To illustrate the importance of the exact structure of the noise in a reduced model we consider the slightly different coupled multiplicative system

$$\begin{aligned} \dot{z}_1 &= z_1^* z_2 + (\mu_1 + e_{11}|z_1|^2 + e_{12}|z_2|^2)z_1 + \lambda(b^{x_1|y_2} v_1 y_2 v_1 + ib^{y_1|x_2} v_2 x_2 v_2), \\ \dot{z}_2 &= -z_1^2 + (\mu_2 + e_{21}|z_1|^2 + e_{22}|z_2|^2)z_2 + \lambda(b^{x_2|y_1} v_2 y_1 v_2 + ib^{y_2|x_1} v_1 x_1 v_1), \\ \dot{u}_k &= -\frac{ik}{2} \sum_{p+q+k=0} \hat{u}_p^* \hat{u}_q^* + \lambda \delta_{1,k} b^{v_1|x_1 y_2} x_1 y_2 + \lambda \delta_{2,k} b^{v_2|x_2 y_1} x_2 y_1. \end{aligned} \tag{15}$$

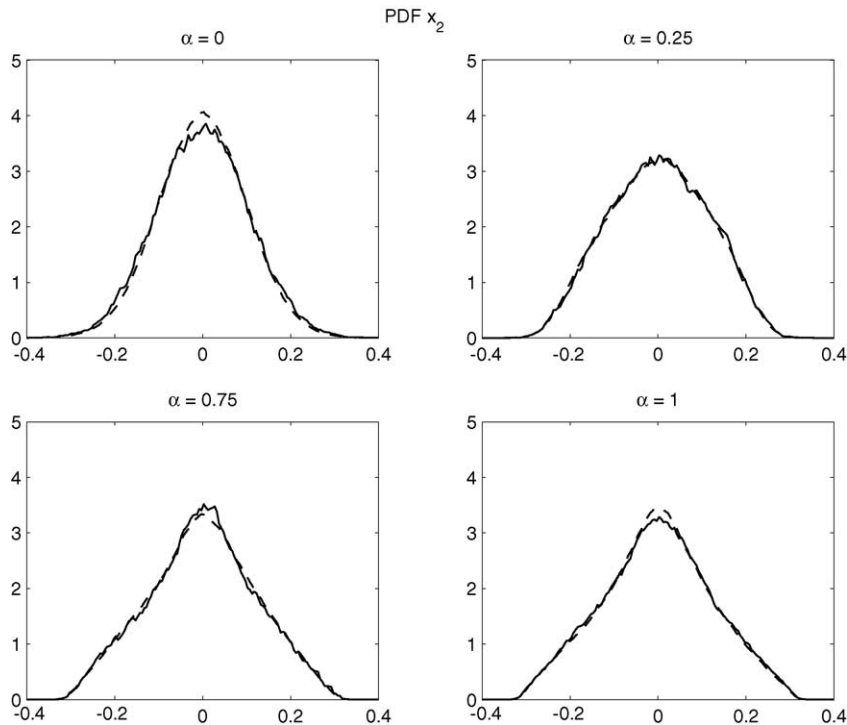


Fig. 22. Marginal PDF of  $x_2$ ; bifurcation with respect to the strength of the nonlinearity in the coupled Additive Model; solid line – full coupled system; dashed – reduced model; two lines overlap on most of the graphs.

Thus, in (15) the two triads which are coupled together are  $x_1, y_2, v_1$  and  $x_2, y_1, v_2$ . The interaction coefficients for the model in (15) are presented in Table 3. We will refer to the multiplicative model in (12) as Type I, and to the multiplicative model in (15) as Type II. A weak noise regime is considered here with  $\lambda = 0.25$  and parameters in (3). In this case, the non-dimensional form of the reduced stochastic equations yields multiplicative noises smaller in strength than the cubic terms (see the explicit non-dimensional form of the multiplicative reduced model of Type I with  $\lambda = 0.25$  in Appendix A). There are a lot of similarities in the statistical behavior of solutions for the two types of multiplicative models, but there are also drastic differences, especially for the one-point statistics of the slow variables,  $z_1$  and  $z_2$ . Comparison of the one-point statistics for the two models is presented in Table 5 and comparison of selected marginal PDFs from two simulations is presented in Fig. 19. While the one-point statistics of  $x_1$  and  $y_1$  are almost the same for the two models, statistical behavior of  $x_2$  and  $y_2$  is very different. The variance of  $x_2$  is almost twice larger for the simulations of Type II model than for the Type I and flatness of  $x_2$  is smaller in the simulations of Type II. One-point statistics of  $y_2$  exhibit the opposite trend. Although the one-point statistics of  $x_1$  and  $y_1$  are nearly identical, the shapes of the marginal PDFs of these variables are very different between the simulations of the two models (cf. left and right columns of Fig. 19). In the simulations of the Type II model the marginal PDF of  $x_1$  has a large peak at  $x_1 = 0$  and two secondary peaks at  $x_1 \approx \pm 0.2$  while for the Type I model the distribution of  $x_1$  is broader with just one maximum at  $x_1 = 0$ . Comparison of joint PDFs for the two models. Although the coupling is weak, there are significant differences between the joint PDFs for the two models. For example, joint PDF  $x_1, x_2$  for Type I multiplicative model in (12) has two peaks at  $(x_1, x_2) = (\pm 0.15, 0)$ . These peaks are absent in the same PDF for Type II model in (15); instead, there is a large peak at  $(x_1, x_2) = (0, -0.3)$ . The orientation of the “cross” in the joint PDF  $x_1, y_1$  is very different for the two types of multiplicative models. In the simulations of the multiplicative model of Type I the “cross” is oriented at  $x_1 = \pm y_1$ , while in the simulations

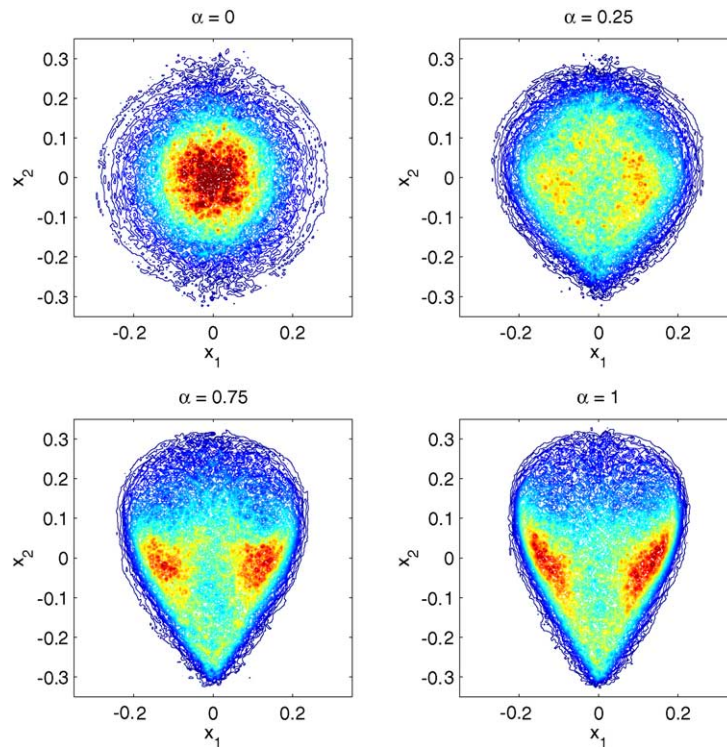


Fig. 23. Joint PDF of  $x_1, x_2$ ; full coupled system.

of the Type II model the orientation is along  $x_1 = 0$ ,  $y_1 = 0$ . These two examples demonstrate that even in a weak coupling limit the detailed specific effects of intrinsic stochastic noise can alter the dynamics in the reduced variables compared with the Monte-Carlo PDFs of the bare chaotic dynamical system presented in Section 3.

## 5. Behavior through the low-dimensional bifurcation sequence

To further address the relationship between the known properties of the projected system of ODEs in (1) and properties of coupled systems we analyze the statistical behavior of the additive model in (4) as parameters  $\mu_{1,2}$  and  $e_{i,j}$  go through a bifurcation sequence of the heteroclinic ODE in (1). We introduce  $\alpha$  as an explicit bifurcation parameter by substituting  $\mu'_{1,2} = \alpha\mu_{1,2}$  and  $e'_{i,j} = \alpha e_{i,j}$  in the equations for  $z_1$  and  $z_2$  in (4). We utilize the same choice of the parameters and interaction coefficients as before (given in (3) and Table 1, respectively) with the strength of coupling equal to one,  $\lambda = 1$ , and bifurcation parameter,  $\alpha$ , varying from zero to one. Thus, regime  $\alpha = 1$  coincides with the simulations described in Section 4.1 with  $\lambda = 1$ . On the other hand, regime  $\alpha = 0$  corresponds to the integrable case for the projected system in (1) mentioned in Section 3. In this case the quadratic terms in (1) conserve the energy  $E = |z_1|^2 + |z_2|^2$  and, in fact, the system in (1) becomes integrable [33] when  $\mu_{1,2} = e_{i,j} = 0$ . Moreover, due to the special property of the coupling coefficients in Table 1, the coupled system in (4) with  $\mu_{1,2} = e_{i,j} = 0$  also conserves energy for the full system,  $E = |z_1|^2 + |z_2|^2 + \sum |u_k|^2$ . The system in (4) also has the Liouville property (volume preserving flow) in this case. Therefore, we can apply the equilibrium statistical mechanics formalism [32,33] and deduce that for  $\alpha = 0$  the most-probable equilibrium state should be Gaussian

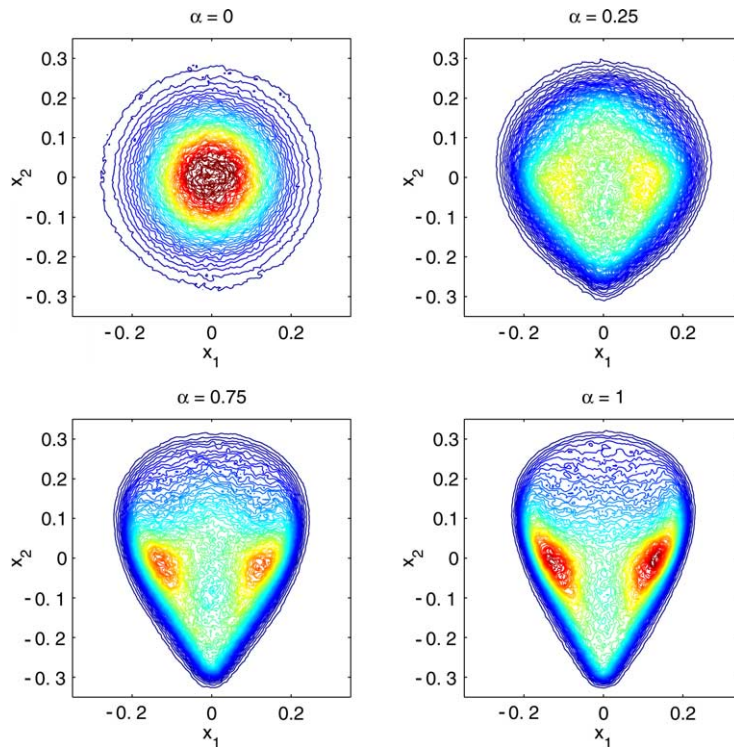


Fig. 24. Joint PDF of  $x_1, x_2$ ; reduced model.

with mean zero and equipartition of energy among all variables

$$P^* = C e^{-\beta(|z_1|^2 + |z_2|^2 + \sum |u_k|^2)}, \quad (16)$$

where parameter  $\beta$  plays the role of the temperature and  $C$  is a normalization constant. Therefore, the limit  $\alpha \rightarrow 0$  of the additive system in (4) is singular in a statistical sense; the behavior of the limiting equations can not be predicted from simulations with  $\alpha > 0$ .

The parameter  $\alpha$  can be easily incorporated into the existence and stability criteria for heteroclinic cycles and periodic motions presented in [3]. For the choice of parameters in (3) heteroclinic cycles exist for all  $0 < \alpha \leq 1$ , but become unstable for  $\alpha \ll 1$ . Instead, periodic and quasi-periodic motion becomes stable for the system of heteroclinic ODEs with small  $\alpha$ . In contrast with the decoupled heteroclinic system in (1), some statistics of the additive model do not exhibit drastic changes when the parameter  $\alpha$  is decreased. For example, the marginal PDFs of the slow variables undergo a very smooth transition. To illustrate this, marginal PDFs of  $x_1$  and  $x_2$  for  $\alpha = 0, 0.25, 0.75, 1$  are depicted in Figs. 21 and 22. Following the existence and stability criteria for the heteroclinic cycles in [3] it is easy to verify that heteroclinic orbits for the system of ODEs in (1) exist for all values of  $\alpha = 0.25, 0.75, 1$ , but for  $\alpha = 0.25$  they are unstable. On the other hand, the stability criteria is satisfied for  $\alpha = 0.75$  and 1. For  $\alpha = 0$ , the truncated system possess a completely different, conservative, behavior as discussed earlier. Figs. 23 and 24 show joint PDFs of  $x_1, x_2$  for the four values of  $\alpha$  (with the same limits and color-coding). For  $\alpha = 0$ , in agreement with the analytical prediction this PDF is Gaussian for both the coupled system and the reduced model. Two-point statistics do not change considerably throughout the bifurcation sequence and are captured by the stochastic mode-reduction technique extremely accurately. While the statistics for simulations with  $\alpha = 0.75$  and 1 is nearly identical, the shape of joint PDFs changes considerably from  $\alpha = 0.25$  to 0.75. The stochastic mode-reduction strategy is able to track the changes in the joint PDFs extremely accurately. Thus, the stochastic mode-reduction strategy can serve as a powerful tool for studying the bifurcation diagrams of complicated high-dimensional models. Even very crude estimates for the stochastic parameters  $\gamma_k$  and  $\sigma_k$  are usually sufficient for reproducing the qualitative behavior of the system. Improved estimates for the stochastic parameters will lead to the correct quantitative picture.

## 6. Concluding remarks

Several prototype models have been introduced here to elucidate the interaction between heteroclinic low-dimensional chaos in projected nonlinear dynamics and intrinsic stochasticity induced by energy exchange with a bath of fast variables. In these models, the truncated nonlinear dynamics with stable heteroclinic cycles is the canonical system of four ODEs arising from 2:1 resonance [3,22] while the chaotic bath of modes is defined by the Galerkin truncated Burgers–Hopf model [32,33,1] with 100 degrees of freedom. These two basic component models are coupled through a variety of elementary energy conserving quadratic nonlinear interactions to define the basic models with both deterministic heteroclinic chaos and intrinsic stochastic chaos on the projected low-dimensional dynamics; this second effect is induced by the back-scatter of energy onto the slow modes. Various types of elementary “additive” and “multiplicative” energy conserving couplings have been studied here which break the symmetry of the heteroclinic chaos. The statistical behavior of the deterministic 104 degrees of freedom system projected on the four-dimensional subspace of slow modes has been compared quantitatively with a four-dimensional stochastic model derived through a systematic stochastic mode-reduction strategy [34–37]; the energy-conserving couplings are classified as “additive” or “multiplicative” according to the nature of the stochastic noise predicted in the stochastic mode reduction theory. More realistic systems in general involve combinations of both types of coupling [34–37].

The following main points have been developed in Sections 3–5 in the present paper:

- (1) The stochastic mode-reduction theory [34–37] which yields a reduced systems of four stochastic DEs for the slow modes reproduces the low-frequency statistical features of the deterministic 104 degrees of freedom

system with remarkable accuracy for all of the parameter regimes and couplings considered in this paper. These statistical features include highly non-Gaussian PDFs, oscillatory time-correlations, and highly non-Gaussian energy-correlations in time as well as their bifurcations with parameters. In fact, the chaotic dynamics in the projected variables enhances the robustness of the stochastic mode-reduction procedure compared with the situation of stable deterministic dynamics for the projected variables [36,37]. Thus, the stochastic mode-reduction technique supplies explicit simplified stochastic models for the nonlinear interaction of heteroclinic chaos with intrinsic stochastic noise.

- (2) The additive interaction models from Section 4.1 demonstrate that the transient behavior of statistical solutions of the projected four-dimensional heteroclinic system is more significant in shadowing the effects of intrinsic stochastic noise in these additive cases than the direct detailed structure of the heteroclinic cycles themselves. It is important to note that while the additive noise levels derived in the stochastic mode-reduction theory are quite small, they are much larger in magnitude non-dimensionally compared with the previous studies of weak additive noise perturbations for heteroclinic ODEs [23,24].
- (3) The multiplicative models in Section 4.2 demonstrate that for these type of couplings, the statistical behavior of ensembles of solutions of the four-dimensional heteroclinic ODEs can completely fail to mimic many of the effects of intrinsic stochastic noise, even when these effects are quite small in magnitude (as for  $\lambda = 0.25$ ). Also properties of the PDFs for the projected variables depend quantitatively on the nature of coupling, even for weak couplings. Nevertheless, these effects are largely captured quantitatively by the systematic reduced stochastic model with four stochastic DEs in both smaller and larger coupling regimes for the deterministic system with 104 degrees of freedom.
- (4) The results in Section 5 indicate that the stochastic mode-reduction techniques are robust through an entire bifurcation sequence of behavior in the deterministic truncated ODEs. Moreover, the stochastic mode-reduction procedure is insensitive to small changes in the statistical properties of the fast variables which makes it a potentially useful tool for qualitative analysis of bifurcations in complex high-dimensional systems with modest separation of time scales. Results of Section 5 demonstrate that it is sufficient to perform direct numerical simulations of the full system only once to estimate statistics of the fast degrees of freedom. After that, the reduced equations for the slow dynamics can be utilized to extrapolate the statistical behavior of the full system for a wide range of parameters.

The models and results in the present paper should provide useful guidelines for the possible behavior in more complex physical systems with many degrees of freedom where there is a competition in their low-frequency variability between low-dimensional chaotic dynamics and intrinsic stochastic chaos due to back-scattering from turbulent cascades. The scenario recently developed in [10] is an excellent starting point and one can envision similar behavior for various regimes of ocean dynamics as well as coupled atmosphere-ocean systems. Recently, the basic stochastic mode reduction strategy used here [34–37] has been simplified for direct practical application in complex climate models and tested in a realistic barotropic model climate on the sphere with orography with very encouraging results [16]. Thus, more practical applications of the strategy used for the paradigm model in the present paper are likely to be developed in the very near future. These are all central topics of further investigation. It is also interesting to study the detailed properties of the four-dimensional reduced stochastic models derived in the present paper.

## Acknowledgments

The authors thank Eric Vanden-Eijnden for his helpful advice during the early stages of this work and Daan Crommelin for his interesting comments. The research of A. Majda is partially supported by NSF Grant DMS-9972865, ONR Grant N00014-96-1-0043, and NSF-CMG Grant DMS02-22133. I. Timofeyev acknowledges support from the NSF through Grant DMS-0405944.

## Appendix A. Non-dimensional reduced equations

### A.1. Additive noise example

The non-dimensionalization of the reduced equations is required to assess the relative magnitude of the noise, linear, and nonlinear terms. A particular example of the non-dimensionalization of the reduced system in (8) for the additive noise coupling from Section 4.1 is presented below. In the first step, new dependent variables are introduced with the requirement that their covariance matrix is the identity. Since in the example from Section 4.1 the covariance matrix of  $x_{1,2}$  and  $y_{1,2}$  is diagonal, this amounts to dividing the dependent variables by square roots of their variances:

$$x_i^{\text{new}} = \frac{x_i}{\sqrt{\text{Var}\{x_i\}}}, \quad y_i^{\text{new}} = \frac{y_i}{\sqrt{\text{Var}\{y_i\}}}. \tag{A.1}$$

In order to avoid cumbersome notation and coefficients it is possible to utilize approximate values for the variances instead of the exact ones from Table 2, i.e.

$$\text{Var}\{x_1\} \approx 0.01 = V_1, \quad \text{Var}\{y_1\} \approx 0.01 = V_1, \quad \text{Var}\{x_2\} \approx 0.016 = V_2, \quad \text{Var}\{y_2\} \approx 0.016 = V_2. \tag{A.2}$$

Substituting (A.1) with the particular values from (A.2) into the equation (8) from Section 4.1 we obtain (the superscript “new” is dropped)

$$\begin{aligned} \begin{pmatrix} x_1 \\ y_1 \end{pmatrix}' &= \begin{pmatrix} \sqrt{V_2}x_1x_2 + \sqrt{V_2}y_1y_2 + x_1(\mu_1 + V_1e_{11}r_1^2 + V_2e_{12}r_2^2) \\ \sqrt{V_2}x_1y_2 - \sqrt{V_2}y_1x_2 + y_1(\mu_1 + V_1e_{11}r_1^2 + V_2e_{12}r_2^2) \end{pmatrix} - A_1(x_1, y_1)^T + \frac{1}{\sqrt{V_1}}\Sigma_1(W_1, W_2)^T, \\ \begin{pmatrix} x_2 \\ y_2 \end{pmatrix}' &= \begin{pmatrix} -\frac{V_1}{\sqrt{V_2}}(x_1^2 - y_1^2) + x_2(\mu_2 + V_1e_{21}r_1^2 + V_2e_{22}r_2^2) \\ -2\frac{V_1}{\sqrt{V_2}}x_1y_1 + y_2(\mu_2 + V_1e_{21}r_1^2 + V_2e_{22}r_2^2) \end{pmatrix} - A_2(x_2, y_2)^T + \frac{1}{\sqrt{V_2}}\Sigma_2(W_3, W_4)^T. \end{aligned} \tag{A.3}$$

Taking into account particular values of  $V_1, V_2$  we obtain the following system of equations:

$$\begin{aligned} \begin{pmatrix} x_1 \\ y_1 \end{pmatrix}' &= \begin{pmatrix} 0.12x_1x_2 + 0.12y_1y_2 + x_1(\mu_1 + 0.01e_{11}r_1^2 + 0.016e_{12}r_2^2) \\ 0.12x_1y_2 - 0.12y_1x_2 + y_1(\mu_1 + 0.01e_{11}r_1^2 + 0.016e_{12}r_2^2) \end{pmatrix} - A_1(x_1, y_1)^T + 10\Sigma_1(W_1, W_2)^T, \\ \begin{pmatrix} x_2 \\ y_2 \end{pmatrix}' &= \begin{pmatrix} -0.08(x_1^2 - y_1^2) + x_2(\mu_2 + 0.01e_{21}r_1^2 + 0.016e_{22}r_2^2) \\ -0.16x_1y_1 + y_2(\mu_2 + 0.01e_{21}r_1^2 + 0.016e_{22}r_2^2) \end{pmatrix} - A_2(x_2, y_2)^T + 7.9\Sigma_2(W_3, W_4)^T, \end{aligned} \tag{A.4}$$

where the values of the damping and forcing matrices are estimated from the direct numerical simulations with  $\lambda = 1$

Table A.1

Estimates for the variance, decay rate of correlations and noise level for the Burgers bath modes  $u_1$  and  $u_2$ 

| $\lambda$ | Var{Re $u_1$ } | Var{Re $u_2$ } | $\gamma_1$ | $\gamma_2$ | $\sigma_1$ | $\sigma_2$ |
|-----------|----------------|----------------|------------|------------|------------|------------|
| 0.25      | 0.01419        | 0.01412        | 0.7072     | 1.5007     | 0.1417     | 0.2059     |
| 0.5       | 0.01491        | 0.01486        | 0.7496     | 1.5039     | 0.1495     | 0.2115     |
| 1         | 0.01272        | 0.01275        | 0.7190     | 1.4687     | 0.1353     | 0.1936     |
| 2         | 0.01316        | 0.01320        | 0.7139     | 1.4083     | 0.1371     | 0.1929     |
| 3         | 0.01285        | 0.01309        | 0.8390     | 1.4616     | 0.1469     | 0.1956     |
| 4         | 0.01218        | 0.01256        | 0.9157     | 1.5359     | 0.1494     | 0.1964     |
| 5         | 0.01184        | 0.01221        | 0.9915     | 1.5637     | 0.1532     | 0.1954     |

$$A_1 = \lambda^2 \begin{pmatrix} 0.0088 & -0.006197 \\ -0.006197 & 0.00433 \end{pmatrix}, \quad A_2 = \lambda^2 \begin{pmatrix} 0.004344 & -0.002389 \\ -0.002389 & 0.001314 \end{pmatrix},$$

$$\Sigma_1 = \lambda \begin{pmatrix} 0.012299 & -0.008609 \\ -0.008609 & 0.006027 \end{pmatrix}, \quad \Sigma_2 = \lambda \begin{pmatrix} 0.009226 & -0.005074 \\ -0.005074 & 0.002791 \end{pmatrix}.$$

Here we use the fact that properties of the fast unresolved modes,  $u_k$ , do not change drastically with  $\lambda$ . This is illustrated in Table A.1 where we present estimates for the statistics of  $u_k$  for several values of  $\lambda$ .

The last step is to rescale time to normalize some terms on the right-hand side to one on average. The form of the reduced equations in A.4 already reveals that the linear, quadratic, cubic terms and noise might be very different in magnitude. We choose to normalize the quadratic terms to be of order one. With this normalization all other heteroclinic terms will be smaller or equal in order. To achieve this we introduce new time variable

$$\tau = 0.1t$$

and keeping in mind that the white noise rescales as the square root of time, i.e.,  $dW(\tau) = \sqrt{0.1}dW(t)$  we obtain the non-dimensional form of the reduced equations:

$$\begin{pmatrix} x_1 \\ y_1 \end{pmatrix}' = \begin{pmatrix} 1.2x_1x_2 + 1.2y_1y_2 + x_1(10\mu_1 + 0.1e_{11}r_1^2 + 0.16e_{12}r_2^2) \\ 1.2x_1y_2 - 1.2y_1x_2 + y_1(10\mu_1 + 0.1e_{11}r_1^2 + 0.16e_{12}r_2^2) \end{pmatrix} - A_1(x_1, y_1)^T + \Sigma_1(W_1, W_2)^T,$$

$$\begin{pmatrix} x_2 \\ y_2 \end{pmatrix}' = \begin{pmatrix} -0.8(x_1^2 - y_1^2) + x_2(10\mu_2 + 0.1e_{21}r_1^2 + 0.16e_{22}r_2^2) \\ -1.6x_1y_1 + y_2(10\mu_2 + 0.1e_{21}r_1^2 + 0.16e_{22}r_2^2) \end{pmatrix} - A_2(x_2, y_2)^T + \Sigma_2(W_3, W_4)^T, \quad (\text{A.5})$$

$$A_1 = \lambda^2 \begin{pmatrix} 0.088 & -0.0619 \\ -0.0619 & 0.0433 \end{pmatrix}, \quad A_2 = \lambda^2 \begin{pmatrix} 0.0434 & -0.0239 \\ -0.0239 & 0.0131 \end{pmatrix},$$

$$\Sigma_1 = \lambda \begin{pmatrix} 0.388 & -0.272 \\ -0.272 & 0.19 \end{pmatrix}, \quad \Sigma_2 = \lambda \begin{pmatrix} 0.23 & -0.127 \\ -0.127 & 0.07 \end{pmatrix}. \quad (\text{A.6})$$

In addition to just comparing the coefficients in Eq. A.5, eigenvalues of  $A_{1,2}$  and  $\Sigma_{1,2}$  provide another measure of the noise strength in the reduced model. The eigenvalues of matrices in (A.6) are

$$\text{Eig}\{A_1\} = 0.132\lambda^2, \quad \text{Eig}\{A_2\} = 0.057\lambda^2, \quad \text{Eig}\{\Sigma_1\} = 0.578\lambda, \quad \text{Eig}\{\Sigma_2\} = 0.3\lambda.$$

## A.2. Multiplicative noise example

Following a similar procedure, the nondimensional multiplicative noise equations from (13) in Section 4.2 are given by

$$\begin{aligned}\dot{x}_1 &= 1.2x_1x_2 + 1.2y_1y_2 + x_1(10\mu_1 + 0.1e_{11}r_1^2 + 0.16e_{12}r_2^2) - 0.122\lambda^2y_1^2x_1 + 0.068\lambda^2x_1 + 0.4528\lambda y_1\dot{W}_1, \\ \dot{y}_1 &= 1.2x_1y_2 - 1.2y_1x_2 + y_1(10\mu_1 + 0.1e_{11}r_1^2 + 0.16e_{12}r_2^2) - 0.041\lambda^2y_1x_1^2 + 0.068\lambda^2y_1 + 0.1508\lambda x_1\dot{W}_1, \\ \dot{x}_2 &= -0.8(x_1^2 - y_1^2) + x_2(10\mu_2 + 0.1e_{21}r_1^2 + 0.16e_{22}r_2^2) - 0.088\lambda^2y_2^2x_2 + 0.031\lambda^2x_2 + 0.3032\lambda y_2\dot{W}_2, \\ \dot{y}_2 &= -1.6x_1y_1 + y_2(10\mu_2 + 0.1e_{21}r_1^2 + 0.16e_{22}r_2^2) - 0.029\lambda^2y_2x_2^2 + 0.031\lambda^2y_2 + 0.1012\lambda x_2\dot{W}_2,\end{aligned}\quad (\text{A.7})$$

where all coefficients in (A.7) are estimated from the direct numerical simulations with  $\lambda = 1$ . Recalling the values of the free parameters given in (3) utilized in the simulations of the coupled systems, we deduce that the multiplicative noise are roughly comparable in magnitude with the cubic terms for the regime  $\lambda = 1$ .

To emphasize the weak noise limit for the simulations in Section 4.2.1 we substitute values of the free parameters in (3) and  $\lambda = 0.25$  in the above equations to obtain the non-dimensional form of the multiplicative Type I model with  $\lambda = 0.25$

$$\begin{aligned}\dot{x}_1 &= 1.2x_1x_2 + 1.2y_1y_2 + x_1(0.5 - 0.4r_1^2 - 0.16r_2^2) - 0.0076y_1^2x_1 + 0.0043x_1 + 0.1132y_1\dot{W}_1, \\ \dot{y}_1 &= 1.2x_1y_2 - 1.2y_1x_2 + y_1(0.5 - 0.4r_1^2 - 0.16r_2^2) - 0.0026y_1x_1^2 + 0.0043y_1 + 0.0377x_1\dot{W}_1, \\ \dot{x}_2 &= -0.8(x_1^2 - y_1^2) + x_2(2 - 0.2r_1^2 - 0.32r_2^2) - 0.0055y_2^2x_2 + 0.0019x_2 + 0.0758y_2\dot{W}_2, \\ \dot{y}_2 &= -1.6x_1y_1 + y_2(2 - 0.2r_1^2 - 0.32r_2^2) - 0.0018y_2x_2^2 + 0.0019y_2 + 0.0253x_2\dot{W}_2.\end{aligned}\quad (\text{A.8})$$

Non-dimensionalization for the multiplicative model of Type II yield qualitatively similar results for the simulations with  $\lambda = 0.25$ .

## References

- [1] R. Abramov, G. Kovacic, A.J. Majda, Hamiltonian structure and statistically relevant conserved quantities for the truncated Burgers–Hopf equation, *Commun. Pure Appl. Math.* 56 (2003) 1–46.
- [2] U. Achatz, G. Branstator, A two-layer model with empirical linear corrections and reduced order for studies of internal climate variability, *J. Atmos. Sci.* 56 (1999) 3140–3160.
- [3] D.J. Ambruster, J. Guckenheimer, P. Holmes, Heteroclinic cycles and modulated traveling waves in systems with O(2) symmetry, *Physica D* 29 (1988) 257–282.
- [4] N. Aubry, P. Holmes, J. Lumley, E. Stone, The dynamics of coherent structures in the wall region of a turbulent boundary layer, *J. Fluid Mech.* (1988) 115–173.
- [5] N. Bloembergen, *Nonlinear Optics*, Benjamin, New York, 1965.
- [6] G. Branstator, S.E. Haupt, An empirical model of barotropic atmospheric dynamics and its response to tropical forcing, *J. Climate* 11 (1995) 2645–2667.
- [7] G.P. Brasseur, J.J. Orlando, G.S. Tyndall (Eds.), *Atmospheric Chemistry and Global Change*, Oxford University Press, 1999.
- [8] J.G. Charney, J.G. DeVore, Multiple flow equilibria in the atmosphere and blocking, *J. Atmos. Sci.* 36 (1979) 1205–1216.
- [9] D.T. Crommelin, Homoclinic dynamics: a scenario for atmospheric ultra-low-frequency variability, *J. Atmos. Sci.* 59 (2002) 1533–1549.
- [10] D.T. Crommelin, Regime transitions and heteroclinic connections in a barotropic atmosphere, *J. Atmos. Sci.* 60 (2003) 229–246.
- [11] T. DelSole, B.F. Farrell, Quasi-linear equilibration of a thermally maintained, stochastically excited jet in a quasigeostrophic model, *J. Atmos. Sci.* 53 (1996) 1781–1797.
- [12] H.E. DeSwart, J. Grasman, Effect of stochastic perturbations on a low-order spectral model of the atmospheric circulation, *Tellus* 39A (1987) 10–24.
- [13] H.A. Dijkstra, M. Ghil, Low frequency variability of the large scale circulation: a dynamical systems approach, *Rev. Geophys.*, in press.
- [14] J. Egger, Master equations for climate parameter sets, *Climate Dynam.* 18 (2001) 169–177.

- [15] J. Egger, K.-P. Hoinka, Covariance analysis of the global atmospheric axial angular momentum budget, *Monthly Weather Rev.* 130 (4) (2002) 1063–1070.
- [16] C. Franzke, A. Majda, E. Vanden-Eijnden, Low order stochastic mode reduction for a realistic barotropic model climate, *J. Atmos. Sci.*, submitted for publication.
- [17] D. Frenkel, B. Smit, *Understanding molecular simulations*, in: *From Algorithms to Applications*, Academic Press, San Diego, 1996.
- [18] C.W. Gardiner, *Handbook of Stochastic Methods*, Springer, Berlin, 1985.
- [19] M. Ghil, A.W. Robertson, “Waves” vs. “Particles” in the atmosphere’s phase space: a pathway to long-range forecasting? *Proc. Nat. Acad. Sci. USA* 99 (2002) 2493–2500.
- [20] J. Guckenheimer, A. Mahalov, Resonant triad interactions in symmetric systems, *Physica D* 54 (1992) 267–310.
- [21] K. Hasselmann, *Stochastic climate models. Part I. Theory*, *Tellus* 28 (1976) 473–485.
- [22] P. Holmes, J.L. Lumley, G. Berkooz, *Turbulence, Coherent Structures, Dynamical Systems and Symmetry*, Cambridge University Press, Cambridge, 1996.
- [23] P. Holmes, E. Stone, Noise induced intermittency in a model of a turbulent boundary layer, *Physica D* 37 (1989) 20–32.
- [24] P. Holmes, E. Stone, Random perturbations of heteroclinic cycles, *SIAM J. Appl. Math.* 50 (3) (1990) 726–743.
- [25] H. Itoh, M. Kimoto, Multiple attractors and chaotic itinerancy in a quasigeostrophic model with realistic topography: implications for weather regimes and low-frequency variability, *J. Atmos. Sci.* 53 (1996) 2217–2231.
- [26] F.-F. Jin, M. Ghil, Intraseasonal oscillations in the extratropics: hopf bifurcation and topographic instabilities, *J. Atmos. Sci.* 47 (1990) 3007–3022.
- [27] R.Z. Khasminsky, *Principle of averaging for parabolic and elliptic differential equations and for Markov processes with small diffusion*, *Theory Prob. Appl.* 8 (1963) 1–21.
- [28] P.E. Kloeden, E. Platen, *Numerical Solutions of Stochastic Differential Equations*, Springer Verlag, New York, 1995.
- [29] T.G. Kurtz, Semigroups of conditioned shifts and approximations of Markov processes, *Ann. Prob.* 3 (1975) 618–642.
- [30] C.E. Leith, Climate response and fluctuation dissipation, *J. Atmos. Sci.* 32 (1975) 2022–2025.
- [31] B. Legras, M. Ghil, Persistent anomalies, blocking and variations in atmospheric predictability, *J. Atmos. Sci.* 42 (1985) 433–471.
- [32] A. Majda, I. Timofeyev, Remarkable statistical behavior for truncated Burgers–Hopf dynamics, *Proc. Nat. Acad. Sci.* 97 (2000) 12413–12417.
- [33] A. Majda, I. Timofeyev, Statistical mechanics for truncations of the Burgers–Hopf equation: a model for intrinsic stochastic behavior with scaling, *Milan J. Math.* 70 (1) (2002) 39–96.
- [34] A. Majda, I. Timofeyev, E. Vanden-Eijnden, Models for stochastic climate prediction, *Proc. Nat. Acad. Sci.* 96 (1999) 14687–14691.
- [35] A. Majda, I. Timofeyev, E. Vanden-Eijnden, A mathematics framework for stochastic climate models, *Commun. Pure Appl. Math.* 54 (2001) 891–974.
- [36] A. Majda, I. Timofeyev, E. Vanden-Eijnden, A priori tests of a stochastic mode reduction strategy, *Physica D* 170 (2002) 206–252.
- [37] A. Majda, I. Timofeyev, E. Vanden-Eijnden, Systematic strategies for stochastic mode reduction in climate, *J. Atmos. Sci.* 60 (14) (2003) 1705–1722.
- [38] B.T. Nadiga, B. Luce, Global bifurcation of Shilnikov type in a double gyre ocean, *J. Phys. Oceanography* 31 (2001) 2669–2690.
- [39] J. Pedlosky, *Geophysical Fluid Dynamics*, 2nd ed., Springer Verlag, New York, 1987.
- [40] C. Schutte, J. Walter, C. Hartmann, W. Huisinga; An averaging principle for fast degrees of freedom exhibiting long-term correlations, *Multiscale Model. Simul.* 2 (3) (2004) 501–526.
- [41] J.A. Whitaker, P.D. Sardeshmukh, A linear theory of extratropical synoptic eddy statistics, *J. Atmos. Sci.* 55 (1998) 237–258.